TECHNISCHE UNIVERSITÄT MÜNCHEN

Fakultät für Medizin

Institut für Medizinische Mikrobiologie, Immunologie und Hygiene

Antigen-dependence of cell cycle speed during priming shapes $CD8^+$ T cell memory

Lorenz Christoph Benjamin Kretschmer

Vollständiger Abdruck der von der Fakultät für Medizin der Technischen Universität München zur Erlangung des akademischen Grades eines

Doktors der Medizinischen Wissenschaft (Dr. med. sci.)

genehmigten Dissertation.

Vorsitzender: Prof. Dr. Jürgen Ruland

Prüfer der Dissertation:

1. Prof. Dr. Dirk Busch
2. Priv.-Doz. Dr. Hendrik Poeck
3. Prof. Dr. Marc Schmidt-Supprian

Die Dissertation wurde am 08.06.2020 bei der Fakultät für Medizin der Technischen Universität München eingereicht und durch die Fakultät für Medizin am 30.12.2020 angenommen.

Parts of this thesis have previously been published:

Kretschmer, L., Flossdorf, M., Mir, J., Cho, Y.-L., Plambeck, M., Treise, I., Toska, A., Heinzel, S., Schiemann, M., Busch, D.H. & Buchholz, V.R. Differential expansion of T central memory precursor and effector subsets is regulated by division speed. *Nature Communications* **11**, 113 (2020).

Table of Contents

1. Introduction 1
1.1. Protection mediated by adaptive immune responses 1
1.2. Mechanisms of pathogen recognition and naïve T cell priming 2
1.3. Time course of the $CD8^+$ T cell response 4
1.4. Regulation of clonal expansion 6
1.5. Insights from in vivo single $CD8^+$ T cell fate mapping 9
2. Aim of this thesis 11
3. Materials and Methods 12
3.1. Materials 12
3.1.1. Chemicals and Reagents 12
3.1.2. Buffers and Media 14
3.1.3. Antibodies 15
3.1.4. Equipment 16
3.1.5. Software 17
3.2. Methods 18
3.2.1. Mice 18
3.2.2. Preparation of cell suspensions from different organs 18
3.2.3. FACS staining procedures for cell surface antigens 19
3.2.4. FACS staining procedures for intracellular antigens 20
3.2.5. Cell cycle analysis 20
3.2.6. Apoptosis measurements 21
3.2.7. Flow cytometric analysis 22
3.2.8. Flow cytometric cell sorting 22
3.2.9. Preparation of peptide-pulsed dendritic cells 23
3.2.10. Bacteria and infections 23
3.2.11. Depletion of dendritic cells and antibiotic treatment 24
3.2.12. Serum measurements of inflammatory cytokines 24
3.2.13. Statistics 24

3.2.14. Computational modeling 24
4. Results 26
4.1. Single $CD8^+$ T cell fate mapping after DC+L.m. vaccination 26
4.2. Investigating cell cycle activity during clonal expansion 28
4.3. Dendritic cell depletion strongly delays the cell cycle of T central memory precursors 31
4.4. Measuring the speed of cell cycle progression in vivo 34
4.5. DNA replication during S phase is delayed in absence of antigenic stimuli 39
4.6. Inflammatory stimuli support faster cycling of effector T cell subsets 40
4.7. Distinct effects of antigen and inflammation on memory $CD8^+$ T cell development 43
5. Discussion 46
5.1. Clonal expansion of $CD8^+$ T cell subsets is regulated by division speed 46
5.2. Reciprocal regulation of cellular differentiation and division speed 47
5.3. Revisiting the autopilot model of antigen-independent T cell proliferation 49
5.4. Versatile role of IL-2 in the development of effector $CD8^+$ T cell subsets 50
5.5. Implications for $CD8^+$ T cell memory and vaccine design 51
6. Summary 53
7. Bibliography 54
8. Acknowledgements 66

Index of Figures

Figure 1: Diversification of an acute CD8$^+$ T cell response. 5

Figure 2: The proliferative output of distinct CD8$^+$ T cell subsets can be regulated by division cessation and/or changes in cell cycle speed. 8

Figure 3: Predicted developmental framework of activated CD8$^+$ T cells from *in vivo* single cell fate mapping. 10

Figure 4: Setup of the single CD8$^+$ T cell fate mapping approach and DC+*L.m.* immunization strategy. 27

Figure 5: Computational modeling based on single CD8$^+$ T cell fate mapping predicts slower proliferation rates of CMPs. 28

Figure 6: Slower cell cycle speed and not premature division cessation distinguishes CMPs from EMPs and TEs. 29

Figure 7: CMPs also adopt slower cell cycle speeds than EMPs and TEs when using a viral vaccination vector. 30

Figure 8: Kinetics of antigen availability during DC+*L.m.* immunization and following DTx treatment at 48 hours. 32

Figure 9: Depletion of antigenic stimuli leads to a pronounced delay in cell cycle progression of CMPs. 33

Figure 10: T cell blast size is not affected by depletion of antigen-presenting DCs. 34

Figure 11: Differences in cell cycle distribution between CMPs and non-CMPs are enhanced upon DC depletion. 35

Figure 12: Cell cycle progression after BrdU-pulsing can be used to discriminate T cells that divide within the observation period. 36

Figure 13: No relevant label uptake occurs beyond 0.5 hours after BrdU-pulsing. 37

Figure 14: Validating the temporal resolution of cell cycle speed measurements. 38

Figure 15: Cell cycle speed of CMPs and non-CMPs is differentially regulated by elongation of G1 and S phase. 39

Figure 16: DNA replication during S phase is delayed in absence of antigenic stimuli. 40

Figure 17: Inflammatory cytokines, but not sustained antigenic stimuli confer enhanced IL-2 responsiveness to non-CMPs via up-regulation of CD25. 41

Figure 18: Enhanced IL-2 responsiveness supports faster proliferation of non-CMPs. 43

Figure 19: Sustained antigen availability during priming, but not inflammation supports strong memory $CD8^+$ T cell responses. 44

Abbreviations

7-AAD	7-Amino-Actinomycin D
ACT	Ammonium chloride-Tris
Amp	Ampicillin
APC	Antigen presenting cell
APC	Allophycocyanin
BHI	Brain heart infusion growth medium
BrdU	5-Bromo-2'-deoxyuridine
BSA	Bovine serum albumin
CD	Cluster of differentiation
CFSE	Carboxyfluorescein succinimidyl ester
CFU	Colony forming units
CMP	Central memory precursor
CM	Central memory
DC	Dendritic cell
DMSO	Dimethyl sulfoxide
DNA	Deoxyribonucleic acid
DTR	Diphtheria toxin receptor
DTx	Diphtheria toxin
EDTA	Ethylendiaminetetraacetate
EdU	5-Ethynyl-2'-deoxyuridine
EMA	Ethidiummonoazid-bromide
EMP	Effector memory precursor
EM	Effector memory

FACS	Fluorescence activated cell sorting
FCS	Fetal calf serum
FITC	Fluorescein-isothiocyanat
FUCCI	Fluorescent ubiquitination-based cell cycle indicator
GFP	Green fluorescent protein
h	hours
IL	Interleukin
IL-7R	Interleukin-7 receptor
IFN-γ	Interferon-γ
i.p.	Intraperitoneal
i.v.	Intravenous
KO	Knockout
L.m.	*Listeria monocytogenes*
L.m.-OVA	*Listeria monocytogenes* expressing Ovalbumin
MHC	Major histocompatibility complex
min	minutes
MP	Memory precursor
MVA-OVA	Modified Vaccinia Ankara expressing Ovalbumin
NA	Nucleoside analogue
OD_{600}	Optical density measured at wavelength of 600nm
OVAp	SIINFEKL-peptide of chicken ovalbumin

PAMP	Pathogen associated molecular pattern
PBS	Phosphate buffered saline
PE	Phycoerythrin
PE/Cy7	Phycoerythrin-Cyanine7
PerCP/Cy5.5	Peridinin-chlorophyll proteins-Cy5.5
PFA	Paraformaldehyde
PFU	Plaque forming units
PI	Propidium iodide
p.i.	Post infection
p:MHC-I	peptide:MHC-I
p-Rb	phosphorylated Retinoblastoma protein
pSTAT5	phosphorylated Signal transducer and activator of transcription 5
Rag	Recombination activating gene
RBC	Red blood cell
rpm	Rounds per minute
RT	Room temperature
SC^+	SC^+ medium supplement
SPF	Specific pathogen-free
TCR	T cell receptor
TE	Terminal effector
TNF-α	Tumor necrosis factor-α
wt	Wild type
wt-*L.m.*	Wild type *Listeria monocytogenes*

1. Introduction

1.1. Protection mediated by adaptive immune responses

Throughout evolution, the mammalian immune system has developed intricate mechanisms to detect the presence of disease-causing pathogens and combat infectious diseases. Innate immune defense generally involves the broad recognition of conserved microbial patterns, coupled to the swift execution of various effector functions. In contrast, protection mediated by adaptive immune responses encompasses highly specific, targeted response mechanisms as well as the generation of long-lived immunological memory (Fearon et al., 1996; Iwasaki et al., 2015). This latter feature characterizes the immune system's ability to adjust after each encounter with harmful microorganisms. Subsequent responses to previously encountered pathogens thus typically elicit stronger and more rapid defense mechanisms. The basis for this state of enhanced protection is formed by specialized memory immune cells, which are maintained after successful resolution of an infection for prolonged periods of time and sometimes up to the whole lifetime of an individual (Sprent et al., 2002).

In general, two broad classes of immune responses are constituted by distinct lineages of the adaptive immune system: *humoral immunity* - driven by B cells, and *cell-mediated immunity*- driven by T cells. While activated B cells secrete soluble antibodies that can neutralize extracellular pathogens or toxins (Strugnell et al., 2010), T cells are able to provide diverse effector functions by releasing inflammatory cytokines or through direct cell-cell interactions. Helper ($CD4^+$) T cells thereby regulate or support the immune function of other cell types (Reiner, 2007), whereas cytotoxic ($CD8^+$) T cells directly kill infected or malignant target cells (Russell et al., 2002). Thus, successful clearance of intracellular pathogens, such as bacteria or viruses (Williams et al., 2007), but also of various tumors (Klebanoff et al., 2006) strongly depends on the efficient generation of protective $CD8^+$ T cell responses. An improved understanding of the mechanisms regulating $CD8^+$ T cell effector functions and memory development therefore continues to present an appealing goal for future vaccine design (Sallusto et al., 2010) and T cell immunotherapy (Appay et al., 2008; Rosenberg et al., 2008).

1.2. Mechanisms of pathogen recognition and naïve T cell priming

During lymphocyte development, a vast diversity of antigen receptors is generated, which mediate the recognition of invading pathogens. In order to mount a targeted immune response against a plethora of different microorganisms, a great breadth of receptor specificities is needed (Goldrath et al., 1999). This is achieved through a unique combinatorial process that equips each developing lymphocyte with an individual B cell receptor or T cell receptor (TCR), respectively (Tonegawa, 1985). While both types of lymphocytes originate from multipotent hematopoietic stem cells in the bone marrow, TCR recombination occurs in the thymus. Within this central lymphoid organ, T cell precursors (thymocytes) are guided by sequential interactions with their microenvironment. Thereby, a process is initiated through which an individual TCR gene sequence is assembled by near random recombination of somatic DNA fragments. Upon expression of a functional TCR on the cell surface and interaction with self-peptide/major histocompatibility complex (MHC) on thymic epithelial cells, recombination is stopped (Starr et al., 2003). This ensures that each thymocyte usually only expresses copies of the same individual TCR, thereby conferring antigen-specificity on a cellular level. In order to accommodate a great breadth of different specificities within a limited cellular repertoire, the frequency of naïve T cells specific for a single epitope is usually low, due to homeostatic restrictions (Blattman et al., 2002). After completion of thymic development, mature naïve T cells are released into the circulation. In the absence of infection, these cells continuously recirculate between the blood and secondary lymphoid organs, such as the lymph nodes and the spleen. Within the microarchitecture of these anatomical sites, naïve T cells first become activated.

Although a variety of different host cells can be naturally infected, not all of these cell types possess the ability to prime an adaptive $CD8^+$ T cell response. Specialized immune cells are required that utilize complex pathways, needed to detect and process pathogenic microorganisms. The most potent activators of T cells are dendritic cells (DCs), named after their characteristic morphological cytoplasmic processes (Steinman, 1991). This cell type can be found in almost all peripheral tissues, where they perform endocytosis and scan their surroundings for pathogen associated molecular patterns (PAMPs). Following infection, antigen is taken up, processed, and loaded as oligopeptides onto MHC molecules: antigen, derived from pathogens that replicate in the cytoplasm, is targeted to MHC-I molecules. Conversely,

extracellular antigen is acquired through endocytosis and is usually loaded onto MHC-II molecules. Moreover, DCs sometimes exploit a specialized process to present certain extracellular antigens in the context of MHC-I. This applies particularly to fragments of infected dead cells that are shuttled into the conventional MHC-I pathway. Through this process, known as cross-presentation, the requirement for the antigen presenting cell (APC) to be directly infected can be bypassed. Finally, peptide loaded MHCs are transported to the cell surface where they are presented to other immune cells (Heath et al., 2004). The recognition of PAMPs, predominantly by ligation with toll-like receptors, additionally induces DC maturation (Akira et al., 2003). This culminates in the up-regulation of MHC expression as well as other co-stimulatory molecules and down-regulation of endocytosis. Mature DCs eventually migrate to secondary lymphoid organs, where they encounter and activate naïve T cells.

Full-fledged activation of naïve $CD8^+$ T cells generally requires the integration of multiple activating signals: recognition of cognate antigen through the TCR (*Signal 1*), co-stimulation (*Signal 2*), both of which are provided by antigen-presenting DCs, and infection-driven inflammatory cytokines (*Signal 3*). The recognition of antigen by $CD8^+$ T cells is generally restricted to peptide-fragments that are presented in the context of MHC-I molecules (p:MHC-I) (Zinkernagel et al., 1974a; Zinkernagel et al., 1974b). On a cellular level, specificity is mediated by selective stimulation of only those T cell clones within the naïve repertoire that harbor an appropriate TCR, recognizing a given p:MHC-I complex (Clonal selection) (Burnet, 1959). Efficient recruitment of these cells is dependent on excessive sampling of antigen-presenting cells in lymphoid organs, estimated to involve 100 different DCs per hour. Likewise, an individual DC is able to establish up to 2.000 cell contacts per hour and engage more than ten T cells simultaneously (Beltman et al., 2007; Bousso et al., 2003). Once an appropriate TCR stimulus is transduced, the activating signal must be further amplified by the co-stimulatory interaction of CD28 molecules with CD80 or CD86 on mature DCs. The lack of co-stimulation results in defective activation and T cell anergy, a state of unresponsiveness to further antigenic stimulation (Sharpe et al., 2002). While activation via *Signal 1* and *2* is generally sufficient for inducing multiple rounds of cell division, instruction for sustained proliferation and full acquisition of effector functions is dependent on the additional presence of *Signal 3*. Various cytokines are able to supply this activating stimulus, including interferon-α/β and interleukin-12 (IL-12) (Mescher et al., 2006). Their induction strongly depends on the nature of the infection or

vaccination, interferon-α/β being predominantly produced during viral- and IL-12 during bacterial infections (Cousens et al., 1999). In addition, both cytokines can be induced by adjuvants, either in vaccine formulations or as a supplement in immunization strategies to augment $CD8^+$ T cell responses (Cui et al., 2009).

1.3. Time course of the $CD8^+$ T cell response

Following activation, $CD8^+$ T cell responses can be typically characterized by the succession of three distinct phases: clonal expansion, contraction, and memory maintenance (Figure 1a). During the expansion phase, antigen-specific $CD8^+$ T cells undergo as many as 15-20 rounds of cell division and acquire potent effector functions. This process culminates in a vast amount of antigen-specific cells 7-8 days after infection that are able to control the invading pathogen. Following resolution of the infection, ~90-95% of this expanded T cell population succumb to apoptosis (contraction), while the remaining ~5-10% form the pool of long-lived memory cells (Lanzavecchia et al., 2000; Williams et al., 2007).

Although the underlying biological mechanisms that determine these drastic differences in cell fate remain elusive, it is now recognized that diverse subsets of $CD8^+$ T cells cooperate, which possess distinct capacities for memory or terminal-effector differentiation (Figure 1b): memory precursors (MPs) display increased expression of the interleukin-7 receptor (IL-7R/CD127), and can be readily detected within the dividing $CD8^+$ T cell population during the early stages of clonal expansion (Huster et al., 2004; Kaech et al., 2003). Signaling via the IL-7R mediates up-regulation of anti-apoptotic molecules, such as Bcl-2, and is essential for homeostatic memory maintenance (Schluns et al., 2000). In addition, memory T cells undergo slow homeostatic turnover in response to basal interleukin-15 (IL-15) (Ku et al., 2000; Zhang et al., 1998), but do not require further antigenic stimulation via their TCR (Lau et al., 1994). Co-stimulatory molecules, like CD27 have also been implicated in memory T cells development (Hendriks et al., 2000) and show strong co-regulation with CD127 (Hikono et al., 2007; Kaech et al., 2003). On the basis of homing receptors, at least two subsets of MPs can be distinguished (Buchholz et al., 2016; Obar et al., 2010a): central memory precursors (CMPs), characterized by increased expression of L-selectin (CD62L) as well as CCR7, and effector memory precursors (EMPs), lacking this expression pattern. After the resolution of an acute infection, central memory (CM)

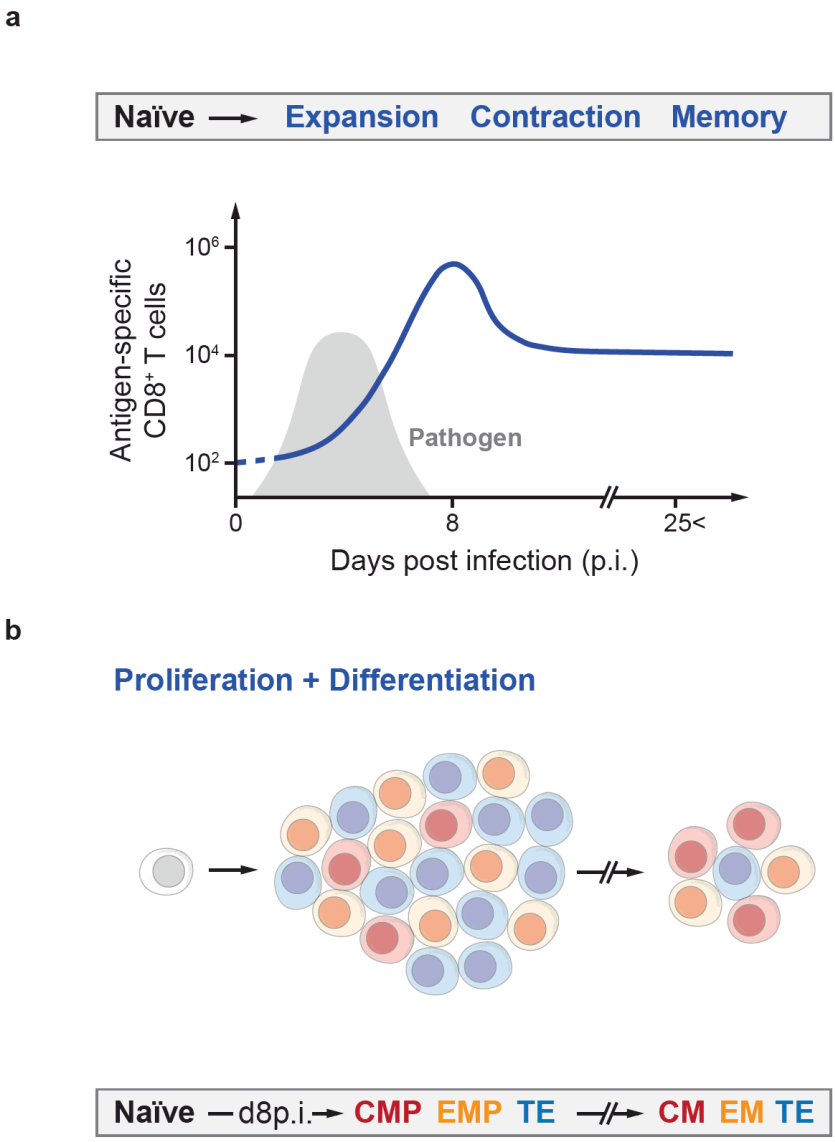

Figure 1 | Diversification of an acute CD8⁺ T cell response. a. Graphical illustration depicting the population size of antigen-specific CD8⁺ T cells (blue line) during the clonal expansion, contraction, and memory phase, upon infection with an invading pathogen (grey). **b**. Schematic representation of the proliferative response, mounted by activated CD8⁺ T cells, and their parallel differentiation into central memory precursor (CMP), effector memory precursor (EMP) and terminal effector (TE) cells towards the peak of the primary immune response. The preferential persistence of central memory (CM) and effector memory (EM) T cells during the memory phase is shown (Modified from: Williams and Bevan, 2007; Kaech et al., 2012).

cells (like naïve T cells) can utilize these cell adhesion molecules to enter and patrol secondary lymphoid organs, the sites of predominant antigen presentation. In contrast, effector memory (EM) cells use various integrins and chemokine receptors to re-locate into inflamed peripheral tissues, such as the lung, liver or gut (Sallusto et al., 1999). Moreover, T-CM cells display a

superior capacity for long-term *in vivo* persistence (Wherry et al., 2003). Upon re-activation during secondary infections, these cells respond with rapid proliferation and give rise to terminal effector cells, whereas T-EM cells undergo much weaker proliferation, but are able to exert immediate effector functions (Sallusto et al., 2004). Collectively, these memory T cells thus provide efficient protection from re-infection.

Throughout the course of a primary $CD8^+$ T cell response, MPs can be further segregated from short-lived terminal effector (TE) cells. Even though this subset retains IL-15 sensitivity, this does not suffice to mediate homeostatic turnover or survival (Joshi et al., 2007). TEs generally lack expression of memory-markers, such as CD127 and CD27, and are destined to undergo apoptosis during the contraction phase (Van Parijs et al., 1998). Conversely, they express high levels of gene transcripts associated with migration, proliferation or various effector functions, including Granzyme A, lysozyme and Fas-ligand, that are crucial for killing infected target cells (Sarkar et al., 2008). This acute immune response can mediate effective pathogen clearance, but can sometimes also entail severe tissue damage, as evidenced by the extensive immunopathology observed in various infections with non-cytopathic viruses, such as hepatitis B and C (Bertoletti et al., 2000).

Taken together, naïve T cell priming induces strong proliferation and differentiation into armed effector subsets that dominate an expanded T cell population around the peak of the response, as well as a much smaller population of long-lived CMPs. How the crucial balance between these acutely and long-term protective $CD8^+$ T cell subsets is achieved during a primary immune response still remains insufficiently understood.

1.4. Regulation of clonal expansion

A tightly regulated cell cycle is crucial for enabling the clonal expansion of antigen-specific $CD8^+$ T cells, thereby ensuring that sufficient numbers of activated daughter cells accumulate that can protect the host from the immediate, but also potentially recurring pathogenic threat. The emergence of distinct $CD8^+$ T cell subsets is thought to begin during the earliest stages of a primary $CD8^+$ T cell response (Arsenio et al., 2014; Buchholz et al., 2013a; Joshi et al., 2007; Kakaradov et al., 2017). However, the striking numerical dominance of effector subsets (non-CMPs) over CMPs only develops much later, towards the peak of the response.

The precise mechanisms leading to this highly disparate expansion of CMPs and non-CMPs have so far not been resolved. Interestingly, it has been suggested that the adoption of subset-specific differences in proliferation activity between emerging CMPs and non-CMPs, over time, mediates a relative outgrowth of the non-CMP compartment (Buchholz et al., 2016). In principle, such regulation could be achieved on two complementary layers: the overall fraction of actively-dividing cells within an antigen-specific $CD8^+$ T cell population (Figure 2a) and/or changes in cell cycle speed (Figure 2b).

Elegant *in vitro* studies have initially demonstrated that primed $CD8^+$ T cells complete up to eight rounds of rapid cell divisions, following as little as two hours of antigenic stimulation (Kaech et al., 2001; van Stipdonk et al., 2001). Moreover, recent reports have suggested that T cell priming imprints a cell-intrinsic, heritable division timer, depending on the nature and strength of initial activation (Marchingo et al., 2014; Marchingo et al., 2016). Primed T cells thereby undergo variable periods of homogenous cell-cycling before abruptly reverting to a quiescent state. A key molecular determinant of this timed division-cessation was found to be abundance of the transcription factor c-Myc (Heinzel et al., 2017). This programed division activity can be prolonged in the presence of inflammatory cytokines (Marchingo et al., 2014), by enhancing responsiveness to the T cell growth factor interleukin-2 (IL-2) (Starbeck-Miller et al., 2014). However, it remains to be determined, in how far this programed division cessation operates within expanding MP and TE populations *in vivo*, where activating stimuli are thought to persist throughout larger parts of the expansion phase.

Intriguingly, recently-activated $CD8^+$ T cells have further been described to adopt very rapid inter-division times of only 6-8 hours, as measured by continuous imaging (Dowling et al., 2014; Kinjyo et al., 2015). They thereby rank among the fastest-cycling cell types of the mammalian organism. In addition, cell cycle speed is not fixed, but can vary depending on the type of infection or vaccination (Yoon et al., 2010). Adoption of shorter cell cycles may either involve accelerated progression through G1 (Yoon et al., 2010) or all phases of the cell cycle, similarly (Dowling et al., 2014). Substantial evidence now indicates that the segregation of MP and TE fates begins shortly after $CD8^+$ T cell priming and should thus occur during a period of very rapid cell-cycling (Arsenio et al., 2014; Badovinac et al., 2005; Joshi et al., 2007; Kakaradov et al., 2017). In line with this notion, timed deuterium-labelling has demonstrated that human memory $CD8^+$ T cells originate from precursors that strongly divided during the first two weeks

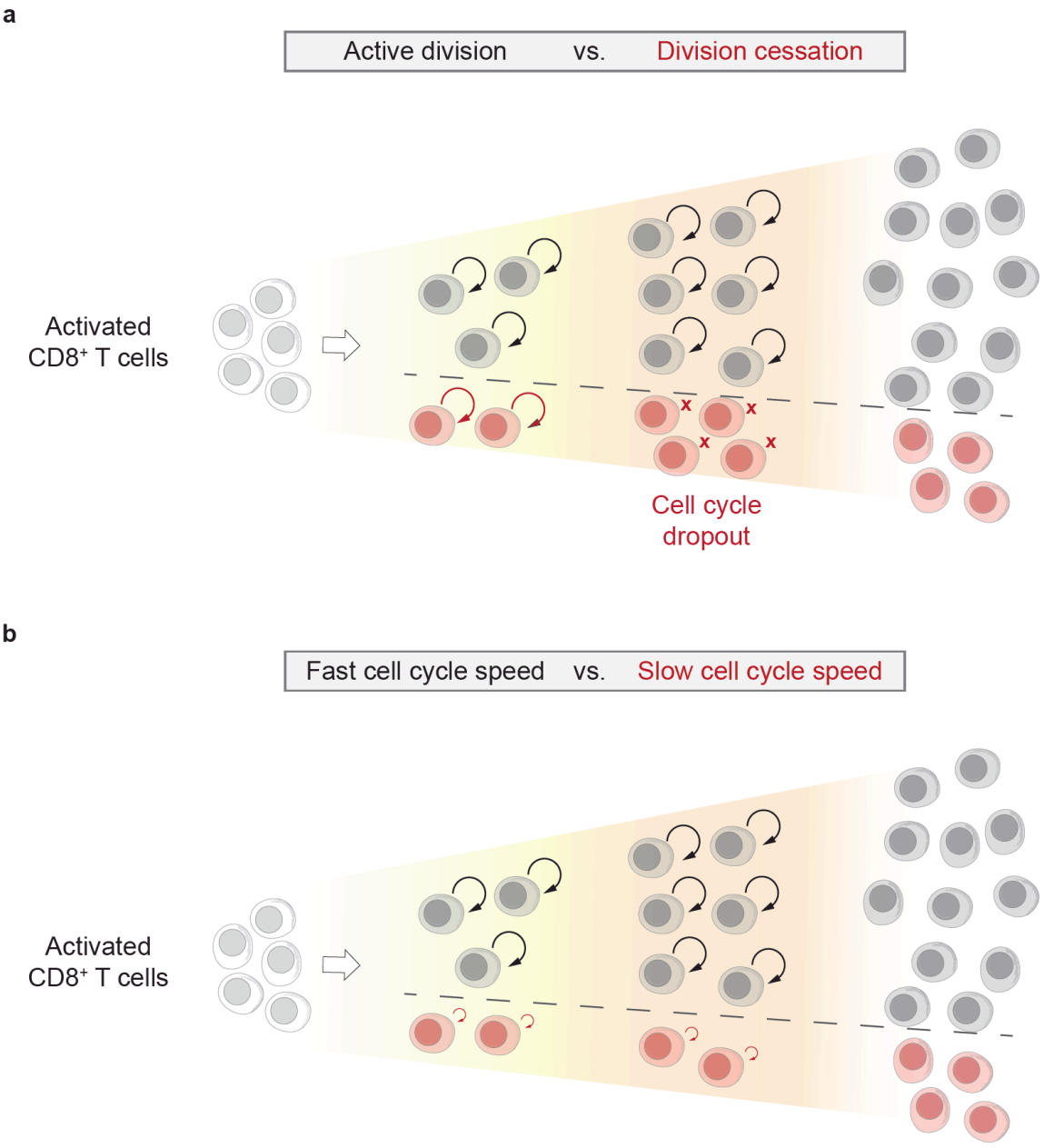

Figure 2 | The proliferative output of distinct CD8⁺ T cell subsets can be regulated by division cessation and/or changes in cell cycle speed. a-b. Graphical illustration depicting the segregation of activated CD8⁺ T cells (left) into two subpopulations, characterized by distinct proliferation activities (middle), and their respective proliferative output after two consecutive rounds of cell division (right). **a.** One subpopulation maintains an actively-dividing state (grey cells, upper branch), whereas another undergoes premature cell cycle dropout after one division (red cells, lower branch). **b**. As in **a**, but for segregation into fast- (grey cells, upper branch) and slow-cycling subpopulations (red cells, lower branch). Dashed lines indicate the segregation between the distinct CD8⁺ T cell subpopulations. Curved arrows indicate active cell divisions, „x" indicates division cessation, larger and smaller curved arrows denote fast and slow cell cycle speeds, respectively.

of yellow fever vaccination (Akondy et al., 2017). Whether the cell cycle speed of these emerging MPs varied from that of TEs during this period could, however, not be resolved. In

murine infection models, MPs were in fact reported to proliferate more weakly than TEs, but only during the later stages of the expansion phase (Sarkar et al., 2008). This finding could be compatible with an earlier division cessation of MPs, but also slower cell cycle speeds. Interestingly, a recent study found that all primed $CD8^+$ T cells initially underwent homogeneous rapid proliferation, before separating into slower-cycling MP and faster-cycling TE subpopulations around the peak of the response, as assessed by direct *ex vivo* imaging (Kinjyo et al., 2015).

Finally, it should be considered that the temporal availability of antigen and inflammation can modulate the fate decision of activated $CD8^+$ T cells, thereby influencing the magnitude of clonal expansion as well as memory T cell development (Blair et al., 2011; Haring et al., 2006; Harty et al., 2008; Prlic et al., 2006). Whether and how the proliferation activities of MPs or TEs are regulated by the presence of these activating stimuli is incompletely understood.

Collectively, MP and TE cells likely emerge during a period of extremely rapid overall cell-cycling, but whether these early fate decisions coincide with the adoption of distinct proliferative behaviors still remains uncertain. In addition, it is unclear in how far the cell cycle activities of distinct $CD8^+$ T cell subsets are influenced by the presence of antigen and inflammation beyond initial T cell priming.

1.5. Insights from *in vivo* single $CD8^+$ T cell fate mapping

Recent advances in single-cell fate mapping approaches have nowadays opened up new avenues for investigating the complex developmental pathways of various immune cell populations (Buchholz et al., 2016). Elegant studies have initially established that both MP and TE cells can be generated from a single antigen-specific $CD8^+$ T cell, responding to an acute bacterial infection *in vivo* (Gerlach et al., 2010; Stemberger et al., 2007). Strikingly, these single cell-derived responses were far from uniform, but instead displayed a strong degree of co-variation between proliferative output and MP or TE differentiation, compared to the highly reproducible response patterns of activated T cell populations. Individual $CD8^+$ T cell families thus encompassed between 10 and 100.000 daughter cells around the peak of a primary immune response, with stronger proliferation critically linked to an increasing abundance of TE over MP cells (Buchholz et al., 2013a; Gerlach et al., 2013).

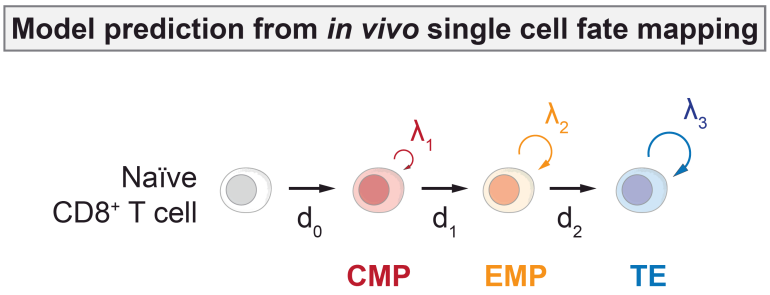

Figure 3 | Predicted developmental framework of activated CD8⁺ T cells from *in vivo* single cell fate mapping. Graphical illustration depicting the differentiation of activated CD8⁺ T cells first into slowly-cycling CMPs, and then into more-rapidly dividing EMPs, and TEs. In this model, d_0-d_2 and λ_1-λ_3 respectively denote the predicted differentiation and proliferation rates for the indicated subsets. A key aspect of this model is the adoption of slower cell cycle speeds by CMPs and faster cell cycle speeds by EMPs and TEs (Modified from Buchholz et al., 2013a).

Remarkably, it has so far remained difficult to disentangle the complex proliferation and differentiation dynamics that unfold in parallel during the clonal expansion phase, by monitoring the response patterns of CD8⁺ T cell populations (Buchholz et al., 2013b). However, applying mathematical modeling to single CD8⁺ T cell-derived responses has recently predicted that MP and TE fates diverge during the earliest stages of the CD8⁺ T cell response and that these fate decisions are subsequently amplified by crucial differences in cell cycle speed during the clonal expansion phase (Buchholz et al., 2013a). This process could be elegantly formalized in a stochastic computational model, in which primed T cells initially differentiate into slowly-cycling CMPs, and then progressively into rapidly-cycling EMPs, and TEs (Figure 3). According to this model, relevant differences in cell cycle speed should therefore act throughout the major parts of the expansion phase and are key to generating the highly-distinct outputs of MPs and TEs towards the peak of the response.

These assumptions thereby challenge the concept that the proliferation activities of MPs and TEs diverge only during the later stages of clonal expansion, but also question the relevance of premature division cessation in these developing T cell subsets. A comprehensive insight into the mechanistic regulation of these crucial developmental processes could moreover be relevant for generating sufficient numbers of MPs or TEs in vaccination settings or for adoptive T cell therapy.

2. Aim of this thesis

Adaptive CD8$^+$ T cell responses to infection or vaccination are characterized by the vigorous proliferation of rare antigen-specific naïve T cells, as well as their differentiation into short-lived effector and long-lived memory subsets. However, the precise developmental pathways underlying the diversification of an antigen-specific CD8$^+$ T cell response remain incompletely understood. In particular, it has been difficult to resolve the complex co-regulation of proliferation and differentiation events during the early stages of clonal expansion (Buchholz et al., 2013b; Buchholz et al., 2016). Thus, it is unclear, whether the emergence of distinct effector and memory CD8$^+$ T cell subsets is accompanied by relevant changes in proliferation activity and when during clonal expansion these changes set in. In principle, such regulation could lie in the acquisition of distinct cell cycle speeds, but also in a differential cessation of division activity within a sub-fraction of responding T cells (Figure 2). In addition, both mechanisms might be influenced by the temporal availability of mitogenic stimuli, such as antigen and inflammation, throughout a primary CD8$^+$ T cell response. An improved understanding of the regulatory circuits leading to an optimal accumulation of acutely and long-term protective CD8$^+$ T cell subsets could be important for the rationale design of effective vaccines as well as adoptive T cell therapy.

<u>The detailed aims of this thesis were to:</u>

1) study the diversification of acute CD8$^+$ T cell responses in a vaccination setup that allows to modulate the availability of antigenic and inflammatory stimuli.
2) use single CD8$^+$ T cell fate mapping to characterize the developmental pathways of memory precursors and effector T cell subsets.
3) measure the proliferation activities of emerging CD8$^+$ T cell subsets directly *in vivo*.
4) investigate the effects of sustained antigenic stimulation and inflammatory cytokines.
5) track memory CD8$^+$ T cell development after curtailing antigenic or inflammatory stimuli.

3. Materials and Methods

3.1. Materials

3.1.1. Chemicals and Reagents

Reagent	Supplier
7-Amino-Actinomycin D (7-AAD)	BD Biosciences, Heidelberg, Germany
Ammonium chloride (NH_4Cl)	Sigma, Taufkirchen, Germany
Ampicillin sodium salt	Carl Roth®, Karlsruhe, Germany
β-Mercaptoethanol	Sigma, Taufkirchen, Germany
Bovine serum albumin (BSA)	Sigma, Taufkirchen, Germany
5-Bromo-2'-deoxyuridine (BrdU)	Sigma, Taufkirchen, Germany
BrdU (10mg/ml in sterile vials)	eBioscience, San Diego, USA
Click-iT™ (Plus) EdU Alexa Fluor™ 647 Flow Cytometry Assay Kits	Thermo Fisher, Darmstadt, Germany
Collagenase from *Clostridium histolyticum*	Sigma, Taufkirchen, Germany
Dimethyl sulfoxide (DMSO)	Sigma, Taufkirchen, Germany
DNase I	Sigma, Taufkirchen, Germany
eBioscience™ BrdU Staining Kit for Flow Cytometry	Thermo Fisher, Darmstadt, Germany
eBioscience™ Fixable Viability Dye eFluor™ 780	Thermo Fisher, Darmstadt, Germany
eBioscience™ Foxp3/Transcription Factor Staining Buffer Set	Thermo Fisher, Darmstadt, Germany
Ethanol	Klinikum rechts der Isar, München, Germany

Reagent	**Supplier**
Ethidiummonoazid-bromide (EMA)	Molecular probes, Leiden, The Netherlands
Ethylendiaminetetraacetic acid disodium salt ($Na_2EDTA*H_20$)	Sigma, Taufkirchen, Germany
Fetal calf serum (FCS)	Biochrom, Berlin, Germany
Gentamycin	Gibco BRL, Karlsruhe, Germany
Hydrochloric acid (HCl_{aq})	Carl Roth®, Karlsruhe, Germany
Heparin-sodium (5000 IU/ml)	Ratiopharm, Ulm, Germany
HEPES	Carl Roth®, Karlsruhe, Germany
Recombinant human IL-2	PeproTech GmbH, Hamburg, Germany
L-Glutamine	Gibco BRL, Karlsruhe, Germany
Methanol (≥99%)	Carl Roth®, Karlsruhe, Germany
Paraformaldehyde (PFA)	Sigma, Taufkirchen, Germany
Penicillin	Carl Roth®, Karlsruhe, Germany
Phosphate buffered saline (PBS)	Biochrome, Berlin, Germany
Propidium iodide (PI)	Invitrogen, Carlsbad, USA
RPMI 1640	PAA, Pasching, Austria
SIINFEKL peptide ($OVA_{257-264}$, 1µg/µl in DMSO)	Biosynthan GmbH, Berlin, Germany
Sodium azide (NaN_3)	Sigma, Taufkirchen, Germany
Sodium chloride (NaCl)	Sigma, Taufkirchen, Germany
Streptomycin	Sigma, Taufkirchen, Germany

Reagent	Supplier
Tris-Hydrochloride (Tris-HCl)	Carl Roth®, Karlsruhe, Germany
Trypan Blue solution	Sigma, Taufkirchen, Germany
Trypsin (1x) gamma irradiated	SAFC Biosciences, Kansas, USA

3.1.2. Buffers and Media

Buffer	Composition
Ammonium chloride-Tris (ACT)	0.17 M NH_4Cl 0.3 M Tris-HCl, pH 7,5
DNAse I working solution	70% FACS buffer, containing 2mM $MgCl_2$ 30% DNAse I stock solution
FACS buffer, pH 7,45	1x PBS 0,5% (w/v) BSA 1,65% (v/v) NaN_3
RP10$^+$ cell culture medium	1x RPMI 1640 10% (v/v) FCS 5% (v/v) SC$^+$
SC$^+$ (medium supplement)	1ml β-Mercaptoethanol 20ml Gentamycin 23,83g HEPES 4g L-Glutamine 200ml Penicillin/Streptomycin

3.1.3. Antibodies

Unless specified otherwise, the following antibodies are directed against mouse antigens and were used at an appropriate dilution, as determined by titration experiments.

Antibody	Clone	Supplier
αBrdU FITC	Bu20a	Thermo Fisher, Darmstadt, Germany
αBrdU Alexa Fluor 488	Mo-BU-1	Thermo Fisher, Darmstadt, Germany
αCD3ε PE	145-2C11	Biolegend, San Diego, USA
αCD8α Pacific Orange	5H10	Thermo Fisher, Darmstadt, Germany
αCD11c eFluor 450	N418	Thermo Fisher, Darmstadt, Germany
αCD16/32 (Fcγ-RII/III; Fc-block)	2.4G2	BD Biosciences, Heidelberg, Germany
αCD19 PE-CF594	1D3	BD Biosciences, Heidelberg, Germany
αCD25 PE	PC61	Thermo Fisher, Darmstadt, Germany
αCD25 APC	PC61	Thermo Fisher, Darmstadt, Germany
αCD27 APC	LG.7F9	Thermo Fisher, Darmstadt, Germany
αCD27 PE	LG.7F9	Thermo Fisher, Darmstadt, Germany
αCD27 PE/Cy7	LG.7F9	Thermo Fisher, Darmstadt, Germany
αCD44 FITC	IM7	Biolegend, San Diego, USA
αCD44 PE-CF594	IM7	BD Biosciences, Heidelberg, Germany
αCD45.1 eFluor 450	A20	Thermo Fisher, Darmstadt, Germany
αCD45.1 FITC	A20	Biolegend, San Diego, USA
αCD45.1 PE	A20	Biolegend, San Diego, USA
αCD45.1 PerCP/Cy5.5	A20	Biolegend, San Diego, USA
αCD45.2 eFluor 450	104	Thermo Fisher, Darmstadt, Germany
αCD62L APC	MEL-14	Biolegend, San Diego, USA
αCD62L FITC	MEL-14	BD Biosciences, Heidelberg, Germany
αCD62L PE	MEL-14	Biolegend, San Diego, USA

Antibody	Clone	Supplier
αCD62L PE/Cy7	MEL-14	Biolegend, San Diego, USA
αCD69 FITC	H1.2F3	Biolegend, San Diego, USA
αCD90.1 APC	HIS51	Thermo Fisher, Darmstadt, Germany
αCD90.1 eF450	HIS51	Thermo Fisher, Darmstadt, Germany
αCD90.1 FITC	HIS51	Thermo Fisher, Darmstadt, Germany
αCD90.2 APC-eFluor 780	53-2.1	Thermo Fisher, Darmstadt, Germany
αc-Myc	D84C12	Cell Signaling, Frankfurt, Germany
αH-2K^{b} bound to SIINFEKL APC	25-D1.16	Thermo Fisher, Darmstadt, Germany
αKi-67 APC	16A8	Biolegend, San Diego, USA
αPhospho-Rb PE (Ser807/811)	D20B12	Cell Signaling, Frankfurt, Germany
αStat5 (pY694) PE	47/Stat5 (pY694)	BD Biosciences, Heidelberg, Germany
Donkey αRabbit IgG PE (minimal x-reactivity)	Poly4064	Biolegend, San Diego, USA

3.1.4. Equipment

Equipment	Model	Supplier
Biological Safety Cabinets	HERAsafe™	Heraeus, Hanau, Germany
Centrifuges	Biofuge fresco	Heraeus, Hanau, Germany
	Multifuge 3 S-R	Heraeus, Hanau, Germany
	Varifuge 3.0RS	Heraeus, Hanau, Germany
Flow Cytometer	Cyan ADP Analyzer	Beckman Coulter, Fullerton, USA
	CytoFLEX LX	Beckman Coulter, Fullerton, USA
	MoFlo Cell Sorter	Beckman Coulter, Fullerton, USA

Equipment	Model	Supplier
Hemocytometer	Neubauer Chamber	Schubert, München, Germany
Incubator	Cytoperm 2	Heraeus, Hanau, Germany
Incubator	Minitron	Infors, Bottmingen, Germany
	BE 500	Memmert, Schwabach, Germany
Microscope	Axiovert S100	Carl Zeiss, Jena, Germany
pH-meter	MultiCal® pH 526	WTW, Weilheim, Germany
Photometer	BioPhotometer	Eppendorf, Hamburg, Germany
Water Bath	LAUDA ecoline 019	Lauda, Königshofen, Germany
Weighing Scale	CP 124 S	Sartorius, Göttingen, Germany

3.1.5. Software

Software	Supplier
Adobe Illustrator 3	Adobe Systems, San Jose, USA
FlowJo (V9.6.4)	Treestar, Ashland, USA
GraphPad Prism (V6.0)	GraphPad Software, La Jolla, USA
Microsoft Office for OS X	Microsoft, Redmond, USA
Summit (V.4.3.02)	Beckman Coulter, California, USA

3.2. Methods

3.2.1. Mice

Female C57BL/6 mice were purchased from Harlan-Winkelmann (now Envigo) at six to eight weeks of age. OTI Rag1$^{-/-}$ Matrix donor mice (Buchholz et al., 2013a) and CD11c-DTR/GFP transgenic mice were bred and maintained under specific pathogen-free (SPF) conditions at the mouse facility of the Technische Universität München. OT1 CD25 knockout mice were bred under SPF conditions at the Walter and Eliza Hall Institute of Medical Research animal facilities (Melbourne, Australia). Animal care and experimental procedures were carried out in accordance with institutional protocols, as approved by the relevant local authorities.

3.2.2. Preparation of cell suspensions from different organs

Leukocyte suspensions from spleen and lymph nodes were prepared by homogenizing whole organs through a 100µm cell strainer into petri dishes (d=5cm) containing 5ml of RP10^{+} medium. After transfer to 15ml falcon tubes, petri dishes were rinsed with an additional 5ml RP10^{+} in order to collect residual cells. Subsequently, red blood cell (RBC) lysis was performed by incubating samples in 3ml ACT buffer (3 minutes at RT) and stopped by adding an excess volume of ice-cold FACS buffer. Cell numbers were determined by counting an appropriate aliquot in a Neubauer chamber, using Trypan Blue to identify and exclude dead cells.
Blood samples of ~100-200µl were collected into heparin-containing 1.5ml Eppendorf Tubes. Optimal RBC lysis was accomplished by stepwise incubation in 10ml ACT (10 minutes at RT) and, after centrifugation and disposal of the supernatant, another 5ml ACT buffer (5 minutes at RT), followed by addition of ice-cold FACS buffer. All samples were then diluted in FACS buffer and further processed for FACS analysis or cell sorting.

3.2.3. FACS staining procedures for cell surface antigens

Antibody staining for FACS analysis was routinely performed in V-bottom 96-well plates at a concentration of 10^7 cells/100µl FACS buffer. In some experiments, total cell numbers of up to $3x10^7$ per sample were stained in separate wells and re-pooled directly before collection to enable the detection of rare events. For blood samples, the whole sample volume was used and typically contained $1\text{-}1.5x10^6$ cells.

Initially, cells were incubated with Fc-block (20 minutes at 4°C) before staining of cell surface antigens, in order to minimize unspecific background fluorescence from binding of antibodies via their Fc portion. For live/dead discrimination, EMA (incubation with Fc-block, under light) or PI (incubation with antibody staining mixture), both of which are DNA-intercalating dyes, were used. Afterwards, cells were washed twice with 100µl and 200µl FACS buffer, respectively. Samples were then resuspended in 100µl FACS buffer containing the particular antibody staining reagents at an appropriate dilution. Every staining procedure further included the preparation of a cell-mixture, pooled from all samples, which was portioned into replicates of ~10^6 cells. One of the replicates was left unstained (except live-dead staining) and was later used to adjust the default fluorescence parameters of the flow cytometer. The remaining replicates were stained with single fluorescent dyes (single color samples), one for each fluorophore used in the respective antibody staining mixture. These single color samples were then used to compensate the partly overlapping emission spectra of the fluorophores. After incubation with the antibody staining mixture (30 minutes at 4°C, in the dark), cells were washed three times with 100µl, 200µl, and 200µl FACS buffer, respectively. If cells were stored before analysis, a 2% PFA solution was added to fix EMA-stained samples at a ratio of 1:1 (storage at 4°C in the dark).

Antibody staining for cell sorting was performed according to the procedures described above, but under sterile conditions, without addition of Fc-block, and a shorter incubation period of the staining mixture (20 minutes at 4°C, in the dark). Cells were washed twice with an excess volume of FACS buffer and PI was added for live/dead discrimination directly before sorting.

3.2.4. FACS staining procedures for intracellular antigens

Antibody staining of transcription factors was performed using the eBioscience™ Foxp3/ Transcription Factor Staining Buffer Set, following the manufacturer's instructions. Briefly, samples were labelled with eBioscience™ Fixable Viability Dye eFluor™ 780 for live/dead discrimination alongside incubation with Fc-block. Cell surface antigens were then stained as described above (Chapter 3.2.3). Afterwards, cells were fixed and permeabilized by incubation in 100µl Fixation/Permeabilization Working Solution (30 minutes at 4°C, in the dark), followed by washing twice with 100µl and 200µl of 1x Perm/Wash Solution, respectively. Subsequently, antibodies directed against the particular transcription factors were added (30min at 4°C, in the dark). For detection of c-Myc, a stepwise staining procedure, consisting of rabbit anti-mouse c-Myc (30 minutes at RT, in the dark) and then fluorophore-labelled goat anti-rabbit (30 minutes at RT, in the dark) was used. Cells were then washed three times with 100µl, 200µl, and 200µl of 1x Perm/Wash Solution, respectively.

In order to measure the IL-2 responsiveness of $CD8^+$ T cell subsets, STAT5 phosphorylation (pSTAT5) was assessed as previously described (Smith et al., 2016). In brief, splenocytes were isolated and, after live/dead staining (Chapter 3.2.3), incubated in a 96-well plate at a concentration of 10^7 cells per 100µl $RP10^+$ (45 minutes, 37°C). Subsequently, titrated amounts of IL-2 were directly added in 100µl pre-warmed $RP10^+$ for 10 minutes. For phospho-flow analysis, samples were immediately transferred to ice and, following centrifugation and disposal of the supernatant, fixed in 100µl of ice-cold 2% PFA solution (10 minutes). In a second step, 900µl ice-cold methanol was directly added and samples were stored at -20°C overnight. Fixed samples were then stained for pSTAT5 or p-Rb together with the particular cell surface antigens (30 minutes at 4°C, in the dark). Before collection, cells were washed three times with 100µl, 200µl, and 200µl FACS buffer, respectively.

3.2.5. Cell cycle analysis

Two distinct nucleoside analogues, EdU and/or BrdU, were used to label dividing cells during S phase transition of the cell cycle. Therefore, 2mg of the reagent was administered i.p. at the

indicated time points, respectively. For the labelling period of 16 hours, 0.8mg/ml BrdU was supplied with 1mg/ml of sucrose via the drinking water.

After organ preparation, samples were immediately stored on ice to inhibit further cell cycle progression *ex vivo*. Every staining procedure typically consisted of $3x10^7$ cells per sample. BrdU incorporation was assessed using the eBioscience™ BrdU Staining Kit for Flow Cytometry, according to the manufacturer's instructions. Briefly, live/dead and cell surface marker staining were performed as described above (Chapter 3.2.3). Afterwards, samples were fixed and permeabilized in 15ml falcon tubes containing 1ml of 1x BrdU Staining Buffer working solution (1-24 hours at RT, in the dark), followed by washing twice with 1ml and 2ml of FACS buffer, respectively. Cells were then incubated with 100µl of DNAse I working solution (1 hour, 37°C, in the dark) in order to expose incorporated BrdU-epitopes, and washed twice with 1ml and 2ml of FACS buffer, respectively. At this point, BrdU was either directly stained with a fluorophore-conjugated antibody (clone Bu20a) or, alternatively, concomitant EdU detection was performed using the Click-iT™ (Plus) EdU Alexa Fluor™ 647 Flow Cytometry Assay Kits, following the procedures specified by the manufacturer. In the latter case, BrdU was stained in a final step by using a non-EdU cross-reactive antibody (clone Mo-BU-1) (Liboska et al., 2012). Samples were washed twice with 1ml and 2ml FACS buffer before collection on a flow cytometer.

In some experiments, total cellular DNA-content was measured by staining samples with 10µl 7-AAD solution (20 minutes at 4°C, in the dark) directly before acquisition. For this, the default settings of the flow cytometer were preset to collect the 7-AAD signal on a linear scale. Apoptotic cells showing a fragmented DNA-content (sub-G1) were excluded from the analysis.

3.2.6. Apoptosis measurements

Identification of dead and apoptotic cells was performed using the eBioscience™ Fixable Viability Dye eFluor 780 and FITC Annexin V Apoptotis Detection Kit (Biolegend, San Diego, USA).

3.2.7. Flow cytometric analysis

Samples were analyzed using a CyAn ADP or CytoFLEX LX flow cytometer (Beckman Coulter, California, USA). Directly before data collection, cell suspensions were filtered through a nylon mesh to remove larger debris. Routinely, between 1-3x10^7 cells were acquired via Summit (v4.3.02, Beckman Coulter, California, USA). FACS data were analyzed using FlowJo software (v9.6.4, Treestar, Ashland, USA).

3.2.8. Flow cytometric cell sorting

T cells for single cell transfer experiments were isolated from peripheral blood of OT-I and OT-I Rag$^{-/-}$ mice via high purity cell sorting on a MoFlo XDP (Beckman Coulter, California, USA), as previously described (Buchholz et al., 2013a). Briefly, donor mice were chosen from eight different congenic backgrounds, ranging from CD90.1/.1-CD45.1/.1 to CD90.2/.2-CD45.1/.2 („OT-I/OT-I Rag$^{-/-}$ Matrix“), which are all distinct from recipient C57BL/6 mice (CD90.2/.2-CD45.2/.2). 1 or 100 naïve CD8$^+$CD44^{low} cells were then sorted (single cell purity mode) into the wells of a V-bottom 96-well plate, containing a pellet of 4x10^5 C57BL/6 splenocytes per 200µl FCS. After successive rounds of single cell sorting each well contained multiple OT-I T cells, distinguishable from each other by their congenic phenotype. Adoptive transfer was performed by administering the whole content of one well i.p.. For the analysis of early time points (i.e. prior to day 8p.i.), larger OT-I T cell numbers were isolated. Therefore, splenocytes from congenic OT-I donor mice were used and naïve T cells were isolated as described above.
For the isolation of DCs, splenocytes from CD11c-DTR/GFP donor mice were used. In these mice, a DTR/GFP transgene is expressed under the CD11c promoter (Jung et al., 2002), which renders CD11$^+$ DCs susceptible to DTx-mediated depletion. FACS Staining was performed in 15ml falcon tubes (20 minutes at 4°C, in the dark). CD11c$^+$ GFP^{high} cells were then sorted (purity mode) after the exclusion of CD3 or CD19-expressing, as well as dead cells, into 15ml falcon tubes containing 1ml FCS. The bulk purity of the target cell population was routinely confirmed to be ≥95%.

3.2.9. Preparation of peptide-pulsed dendritic cells

To efficiently liberate DCs from spleens of CD11c-DTR/GFP transgenic mice, whole organs were aseptically removed and perfused with collagenase solution (0.2mg/ml $RP10^+$ medium), followed by incubation for 30 minutes at 37°C. Spleens were then homogenized through a 100µm cell strainer and further incubated (25 minutes at 37°C), before digestion was stopped with 500µl of 0.1M Na_2EDTA solution. Preparation of cell suspensions and DC sorting were performed as described above (Chapter 3.2.2 and 3.2.8). All preparation steps after cell sorting were performed at room temperature. Highly-pure DCs were resuspended in 1ml $RP10^+$ medium, containing 1µg SIINFEKL peptide, and transferred to a 12-well plate. In order to allow for homogenous peptide-loading, the DC suspension was incubated for 1 hour (37°C), followed by washing twice with 10ml PBS, to remove residual soluble antigen. Finally, cells were resuspended in 1ml PBS and the exact number of viable DCs was determined by acquiring a FACS file of 25µl aliquot that had been re-stained with PI immediately before. According to this measurement, the cell suspension was further diluted in PBS to yield a final concentration of 10^6 cells/200µl.

3.2.10. Bacteria and infections

For bacterial infections, *Listeria monocytogenes* expressing Ovalbumin (*L.m.*-OVA, kindly provided by H. Shen, Philadelphia, USA) or the parental wild type strain 10403S (wt-*L.m.*) were used. The dosages were $2x10^3$ colony forming units (CFU) wt-*L.m.* or $2x10^5$ CFU *L.m.*-OVA in primary or secondary infection experiments, respectively. Bacterial growth was initiated by adding 10µl bacterial glycerol stock to 5ml BHI medium and incubation at 37°C, while gently shaking (90rpm). Once the bacteria had reached the exponential growth phase, as confirmed by OD measurements ($OD_{600} \approx 0.05$), their concentration was estimated from calibration curves using the formula $c=12x10^8xOD_{600}$ CFU/ml. Subsequently, bacteria were diluted to the indicated dosages in sterile PBS and administered i.v.. The infectious dose was controlled by counting CFU from aliquots that had been plated onto BHI plates, after overnight incubation. In some experiments, 10^8 PFU Modified Vaccinia Ankara expressing Ovalbumin (MVA-OVA) were administered i.p.

3.2.11. Depletion of dendritic cells and antibiotic treatment

Depletion of DCs was performed as previously described (Prlic et al., 2006). For antibiotic treatment, 1mg Amp was administered i.p..

3.2.12. Serum measurements of inflammatory cytokines

Mouse serum (~30µl) was obtained by collecting whole blood in sterile 1.5ml Eppendorf tubes at the indicated time points after infection. Samples were then left to clot for 15 minutes at RT, followed by centrifugation and transfer of supernatant to fresh, sterile Eppendorf tubes. Serum was immediately stored at -80°C until analysis (one thaw cycle) in order to avoid degradation (de Jager et al., 2009). Cytokine concentrations were determined using the V-PLEX Plus Proinflammatory Panel 1 Mouse Kit (Meso Scale Discovery, Rockville, USA), following the manufacturer's instructions. Data acquisition and analysis was carried out using the MSD instrument (Meso QuickPlex SQ120) and the included MSD Discovery Workbench 4.0 software.

3.2.13. Statistics

Descriptive statistics and statistical tests were performed with Prism 5.0 for Windows (GraphPad Software, La Jolla, USA), as indicated in the figure legends. In general, D'Agostino-Pearson omnibus normality test was used to first determine if the data was normally distributed. *P*-values were then calculated using one-way ANOVA, Mann-Whitney, and Spearman non-parametric testing. Significance levels amounted to: *$P<0.05$, **$P<0.01$, ***$P<0.001$, ****$P<0.0001$.

3.2.14. Computational modeling

Mathematical modeling and all related model simulations were developed and performed in the group of Dr. Michael Flossdorf at the Technische Universität München, Germany. This effort included devising the conceptual framework for quantifying the duration of the cell cycle, as presented in Chapter 4.4 of this work, as well as extensive validation efforts based on the

experimental data. A detailed account of the computational approaches is given in the Supplementary Information of Kretschmer et al., 2020.

4. Results

4.1. Single CD8$^+$ T cell fate mapping after DC+*L.m.* vaccination

The diversification of acute CD8$^+$ T cell responses can be studied in a variety of bacterial or viral infection models and vaccination schemes. An elegant setup that allows to modulate the efficiency of clonal expansion *in vivo* is based on antigen delivery by peptide-pulsed DCs, expressing a diphtheria toxin receptor (DTR)-transgene under the CD11c promoter (Jung et al., 2002), with an accompanying wild type *Listeria monocytogenes* (wt-*L.m.*) infection (Prlic et al., 2006). In this immunization approach (DC+*L.m.*), diphtheria toxin (DTx)-mediated DC depletion has previously been described to abrogate antigen presentation within 6-12 hours and should not be disturbed by residual cross-presentation on host APCs (Livingstone et al., 2002; Prlic et al., 2006). Since rodent cells naturally lack sensitivity to DTx (Jung et al., 2002), other recipient cells further remain unaffected by this DC depletion.

In order to map the fate of individual CD8$^+$ T cells responding to DC+*L.m.* immunization, naïve T cells were isolated from congenically distinct OT1 TCR transgenic Rag1$^{-/-}$ donor mice (A-H) and transferred into wild type C57BL/6 recipients (R) (Figure 4a). Following a previously established approach (Buchholz et al., 2013a), this transfer in fact consisted of individual cells for congenic matrix phenotypes A-G and a 100-cell control population for phenotype H (Figure 4a and c). On the basis of their unique congenic marker combinations, all transferred OT1 cells (A-H) can be reliably distinguished from one another, as well as the cells of the recipient (R). One day after adoptive transfer, DCs were sorted from spleens of CD11c-DTR/GFP donor mice (Figure 4b, left panel) and subsequently pulsed *in vitro* with SIINFEKL-peptide (OVAp) of the experimental antigen ovalbumin. Directly before injection, purified DCs stained homogeneously positive for OVAp-loaded H-2K^b (MHC-I) molecules on their cell surface (Figure 4b, right panel), which are recognized by CD8$^+$ T cells expressing the OT1 TCR. Following immunization with 10^6 OVAp-pulsed DCs and $2x10^3$ CFU of wt-*L.m.*, immune responses generated by transferred OT1 cells were analyzed in the spleens of recipient mice eight days later (Figure 4c).

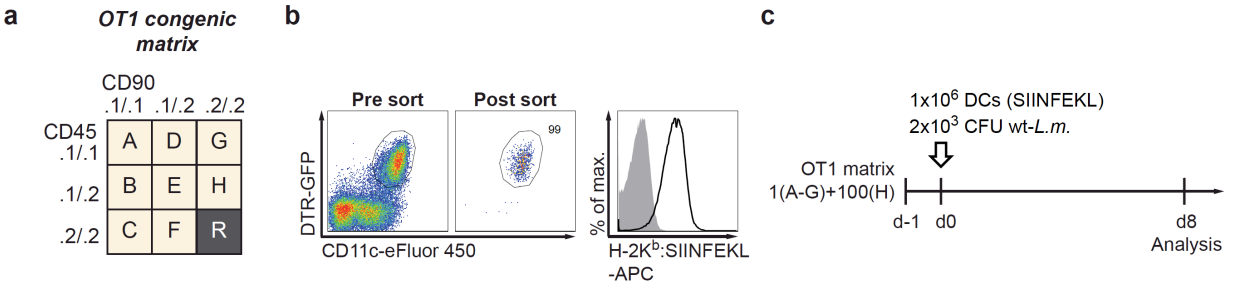

Figure 4 | Setup of the single CD8$^+$ T cell fate mapping approach and DC+*L.m.* immunization strategy. a. Scheme depicting genotypes of OT1 donor mice (A-H), characterized by their unique expression profiles of the congenic markers CD45.1 and CD90.1 (OT1 congenic matrix), which are further distinct from that of C57BL/6 recipients (R). **b**. Representative pseudo-color plots illustrating the sorting strategy for DCs (pre-gated on living CD3$^-$CD19$^-$ cells), with corresponding histogram showing the detection of H-2Kb (MHC-I)-SIINFEKL after peptide-pulsing (grey: isotype control). **c.** Setup of the single cell adoptive transfer system and immunization strategy using SIINFEKL-pulsed DCs and wild-type *L.m.* (modified from Kretschmer et al., 2020).

Progenies could be readily detected for both the single and 100-cell population transfer and showed phenotypic diversification into CMP (CD62L$^+$CD27$^+$), EMP (CD62L$^-$CD27$^+$), and TE (CD62L$^-$CD27$^-$) cells (Figure 5a). The response patterns generated by single OT1 T cells were, however, highly variable, opposed to the much more reproducible patterns of 100-cell-derived responses (Figure 5a and b). Increased expansion of single-cell-derived progenies was moreover found to inversely correlate with the fraction of cells expressing the memory-associated markers CD62L and CD27 (Figure 5c).

Similar results have previously been observed in a recombinant *L.m.*-OVA infection setting (Buchholz et al., 2013a; Gerlach et al., 2013) and have allowed to infer a stochastic computational model that adequately describes the measured expansion and diversification patterns of individual cells as well as the 100-cell control populations (Buchholz et al., 2013a). Such a model, characterized by subset-specific proliferation (λ_1-λ_3) and differentiation rates (d_0-d_2), predicted that naïve T cells first differentiate into CMPs, and then progressively into EMPs, and TEs (Figure 5d). Along progression of this differentiation pathway, cell cycle speed should significantly increase (Buchholz et al., 2013a). Notably, this important feature was recapitulated when applying the published model structure to the data set obtained after DC+*L.m.* immunization, suggesting that CMPs had adopted substantially reduced proliferation rates, compared to their EMP and TE descendants (Figure 5e). However, direct experimental evidence

for this apparent coupling of early T cell fate decisions to immediate changes in cell cycle speed is currently lacking.

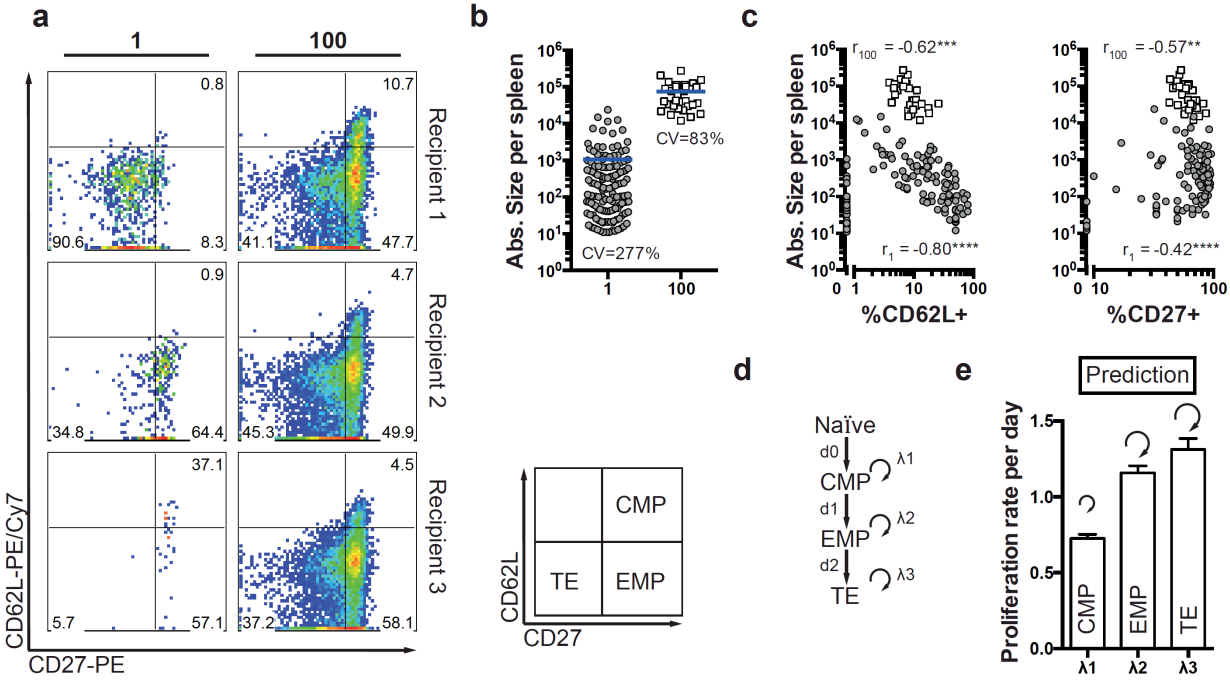

Figure 5 | Computational modeling based on single CD8⁺ T cell fate mapping predicts slower proliferation rates of CMPs. a. Representative pseudo-color plots showing expression of CD27 and CD62L for large to small 1 cell-derived progenies, together with the respective 100 cell-derived progenies in the same recipients. **b.** Scatter plot depicts the absolute number of daughter cells per transferred 1 or 100 cells. **c.** Scatter plots depict the correlation of size and percentage of CD62L (left) or CD27 (right) expressing cells. **d.** Model scheme used for fitting to the experimental data. **e.** Bar graph depicts model prediction of subset-specific proliferation rates (λ_1-λ_3) per day. Lines depict the mean, „CV" indicates the coefficient of variation (**b**). ****$P < 0.0001$, ***$P < 0.001$, **$P < 0.01$ (Spearman non-parametric testing (**c**)). Data are compiled from nine independent experiments (modified from Kretschmer et al., 2020).

4.2. Investigating cell cycle activity during clonal expansion

It has previously been established that CD8⁺ T cells, showing the functional and phenotypic characteristics of prospective memory cells, can be readily detected as early as day 4-6 after DC vaccination (Badovinac et al., 2005). To initially explore the potential differences in cell cycle activity of such MPs and TEs in our DC+*L.m.* immunization approach, expression of the

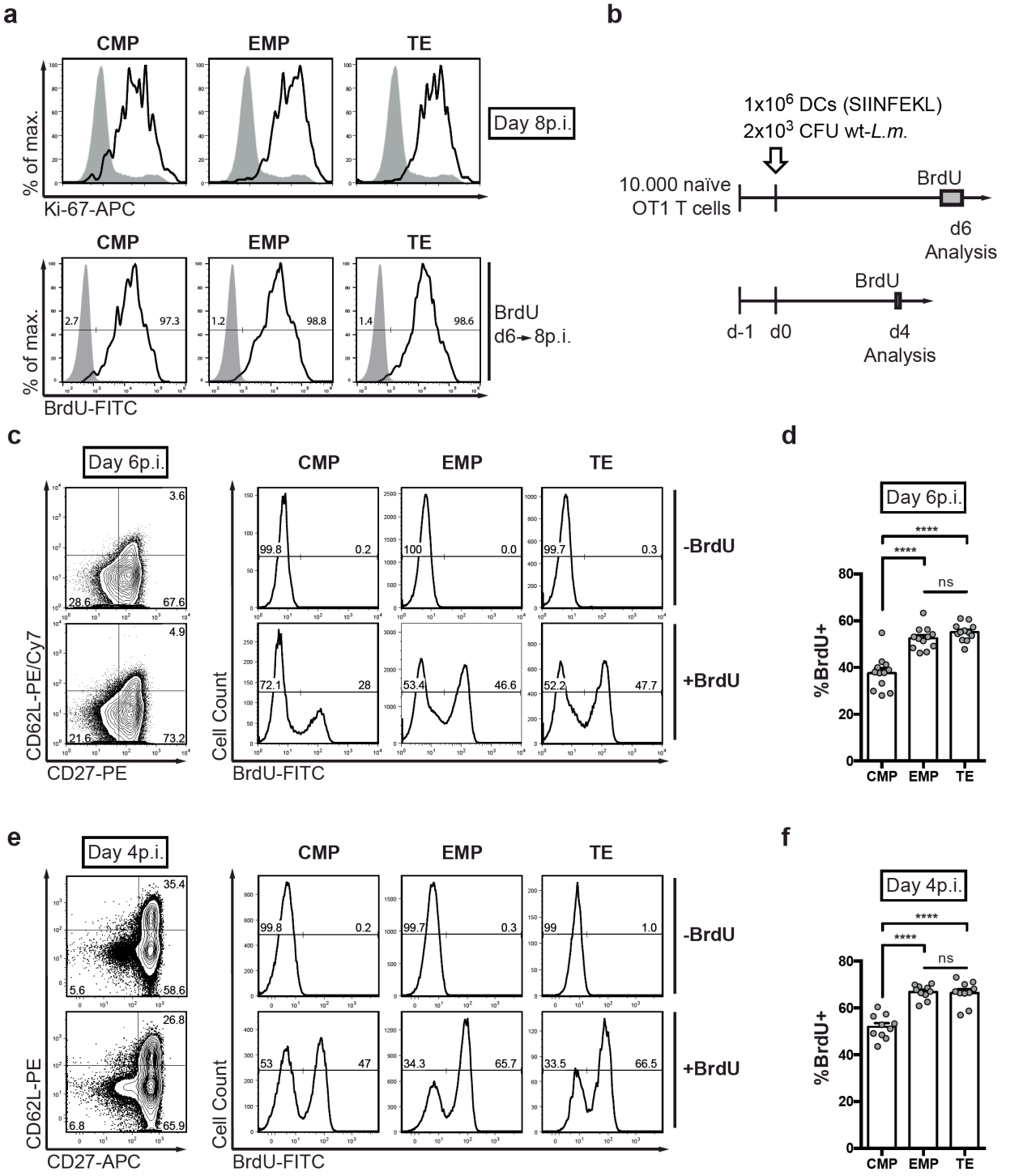

Figure 6 | Slower cell cycle speed and not premature division cessation distinguishes CMPs from EMPs and TEs. a. Progenies were recovered per transferred 100 naïve OT1 cells from spleen at day 8 after DC+*L.m.* immunization. Representative histograms depicting expression of cell cycle-associated Ki-67 (upper row), as well as BrdU uptake (lower row) after repetitive 6h pulses between day 6 and 8p.i. for CMPs, EMPs, and TEs (grey: endogenous naïve $CD8^+$ T cells). **b.** C57BL/6 mice received 10.000 naïve OT1 cells and were immunized with DC+*L.m.* BrdU incorporation into freshly synthesized DNA was analyzed at day 6 or 4 and after 16 or 3 hours of labelling, respectively. **c.** Representative contour plots showing the expression of CD62L and CD27 for transferred T cells, with corresponding histograms showing the BrdU profiles of the indicated subsets at day 6 (upper row: no BrdU administered). **d.** Bar graph depicts the percentage of $BrdU^+$ cells at day 6 (n=12). **e, f.** As in **c** and **d**, but for day 4 (n=10). Naïve cells were excluded for the analysis (pre-gated: $CD44^{high}$). Lines indicate the mean, error bars the s.e.m. ****$P < 0.0001$ (ANOVA). Data are representative of two independent experiments (**a**) or compiled from four (**c, d**) and two independent experiments (**e, f**) (modified from Kretschmer et al., 2020).

proliferation-associated marker Ki67 was evaluated. This protein is up-regulated during all active phases of the cell cycle (Scholzen et al., 2000) (G1, S , G2M - but not G0) and fully degraded with 24-48 hours after division-cessation (Miller et al., 2018). Notably, CMPs, EMPs, and TEs all stained homogeneously positive for Ki67 at day 8, suggesting that all subsets had been actively-cycling beyond day six post immunization (Figure 6a, upper panel). To confirm this assumption, a repetitive BrdU-pulsing approach was used to label cells during S phase progression of their cell cycle between day six to eight. After the labelling period, nearly 100% of cells in all subsets stained positive for BrdU (Figure 6a, lower panel). This meant that almost all CMPs, EMPs, and TEs had in fact continued to cycle through S phase beyond day six.

In view of this apparent lack of premature division cessation, shorter BrdU pulses were subsequently used to inquire into potential differences in cell cycle speed between these subsets (Figure 6b). At day six after immunization, CMPs indeed showed significantly reduced BrdU uptake, compared to EMPs and TEs, within a 16 hour labelling period (Figure 6c and d).

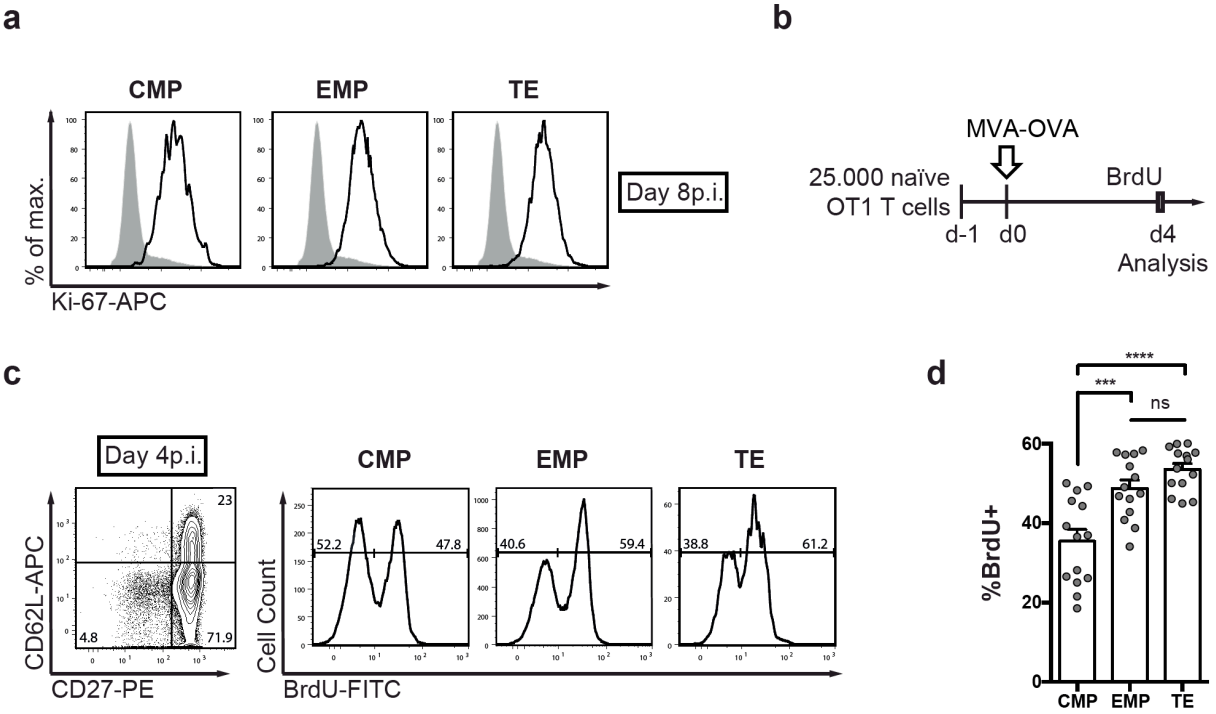

Figure 7 | CMPs also adopt slower cell cycle speeds than EMPs and TEs when using a viral vaccination vector. a. Progenies were recovered per transferred 100 naïve OT1 cells from spleen at day 8 after MVA-OVA immunization. Representative histograms showing expression of cell cycle-associated Ki67 for CMPs, EMPs, and TEs (grey: endogenous naïve $CD8^+$ T cells). **b.** C57BL/6 mice were transferred with $2{,}5x10^4$ naïve OT1 cells and immunized one day later with MVA-OVA. BrdU incorporation was analyzed at day 4, after 3 hours of labelling. **c.** Representative contour plot showing the expression of CD62L and CD27 for transferred T cells, with corresponding histograms showing the BrdU profiles for the indicated subsets. **d.** Bar graph depicts the percentage of $BrdU^+$ cells (n=14). Lines indicate the mean, error bars the s.e.m. $^{****}P < 0.0001$, $^{***}P < 0.001$ (ANOVA). Data are from three independent experiments (modified from Kretschmer et al., 2020).

Remarkably, when analyzing BrdU incorporation at day four and after only 3 hours of labelling, BrdU uptake in all subsets was higher, but CMPs still cycled much slower than EMPs and TEs (Figure 6e and f). Interestingly, this effect was not specific to the applied DC+*L.m.* immunization strategy, as a similar proliferative hierarchy could be observed when using MVA-OVA as an alternative viral vaccination vector (Figure 7).

Collectively, this data indicated that activated $CD8^+$ T cells retained an actively cycling state throughout the larger part of the expansion phase, but had segregated into slowly-cycling CMP and faster-cycling EMP and TE cells already by day four.

4.3. Dendritic cell depletion strongly delays the cell cycle of T central memory precursors

Curtailing antigenic stimuli within 48 hours after DC+*L.m.* immunization has previously been shown to reduce the response magnitude of activated $CD8^+$ T cell populations (Prlic et al., 2006). How the specific cell cycle activities of emerging MP and TE cells are affected by this timed depletion of antigen-presenting DCs has so far not been investigated. To first assess the unperturbed kinetics of antigen availability during DC+*L.m.* immunization, induction of the early activation marker CD69 (Ziegler et al., 1994) was analyzed after transferring naïve OT1 T cell populations at various time points into an ongoing immune response (Figure 8a). Based on this approach, antigenic stimuli remained available for priming of transferred OT1 cells for four to six days after DC+*L.m.* immunization (Figure 8b and d). As expected, this kinetic was, however, severely curtailed following DTx treatment at 48 hours (Figure 8c and d).

When further measuring the subset composition of 100 OT1 T cell-derived populations that had expanded in the absence of sustained antigen presence (Figure 9a), it became clear that absolute cell numbers of all subsets were reduced at the peak of the response (Figure 9b and c). Notably, this reduction most strongly affected CMP and EMP cells (10-fold reduction vs. 5-fold reduction in TEs) (Figure 9c) and thus coincided with a relative polarization of the overall response towards a TE phenotype (Figure 9b). By fitting the previously applied computational model to this data set and retaining the original values for differentiation rates, it was estimated how the proliferation rates of CMPs, EMPs, and TEs should change after DC depletion (Figure 9d). Considering a reported delay in terminating antigenic stimuli after DC depletion (Prlic et al.,

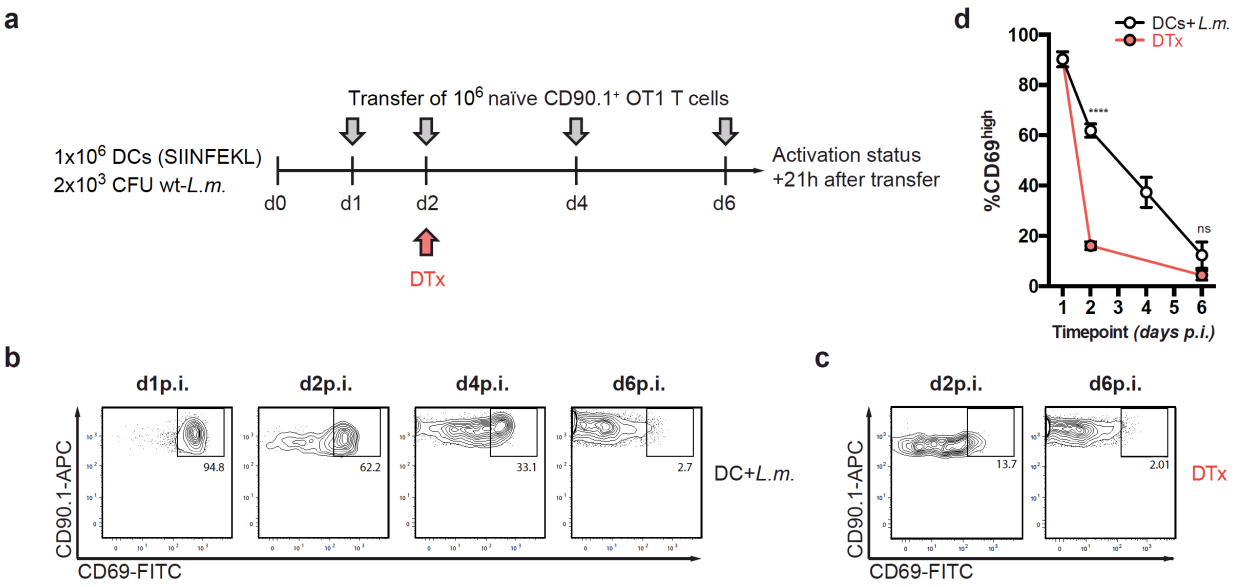

Figure 8 | Kinetics of antigen availability during DC+*L.m.* immunization and following DTx treatment at 48 hours. a. C57BL/6 mice were immunized with DC+*L.m.* and received adoptive transfer of 10^6 naïve OT1 cells (CD90.1$^+$) at the indicated time points post infection. The activation status of transferred OT1 cells was analyzed after 21 hours. One group received DTx treatment at 48 hours p.i. and OT1 transfer 6 hours later (d2) or at day 6 (d6). **b.** Representative contour plots showing expression of CD90.1 and CD69 on transferred OT1 cells 21 hours after the indicated (transfer) time points. **c.** As in b, but following DTx treatment at 48 hours. **d.** Graph depicts the percentage of activated (CD69^{high}) cells among transferred OT1 cells (n=3-4 per time point). Lines indicate the mean, error bars the s.e.m. ****$P < 0.0001$ (t-test). Data are from five independent experiments (modified from Kretschmer et al., 2020).

2006), changes in proliferation rates were thus implemented in the model from 12 hours onwards after DTx treatment. The obtained values for these altered proliferation rates (κ_1-κ_3) suggested that CMPs had markedly slowed down their cell cycle speed in absence of antigen, relative to the DC+*L.m.* control setting, while EMPs and TEs were not as strongly affected (Figure 9e). To directly measure cell cycle progression of these subsets after DC depletion, BrdU incorporation was assessed at day four post vaccination and after 3 hours of labelling. As predicted, CMPs indeed exhibited a pronounced reduction in BrdU uptake in absence of antigen, relative to the untreated group, which was also significantly stronger than for EMPs and TEs (Figure 9f and g). In principle, the identified differences in BrdU-incorporation could again be explained by partial division-cessation, induced by antigen withdrawal, as well as reduced cell cycle speeds. However, all subsets stained positive for highly-acute measures of active cell-cycling, c-Myc (Figure 9h) and hyper-phosphorylated retinoblastoma (Rb) proteins (Figure 9i) (Gookin et al., 2017; Heinzel et al., 2017; Spencer et al., 2013), directly at day four. Unlike Ki-67, these

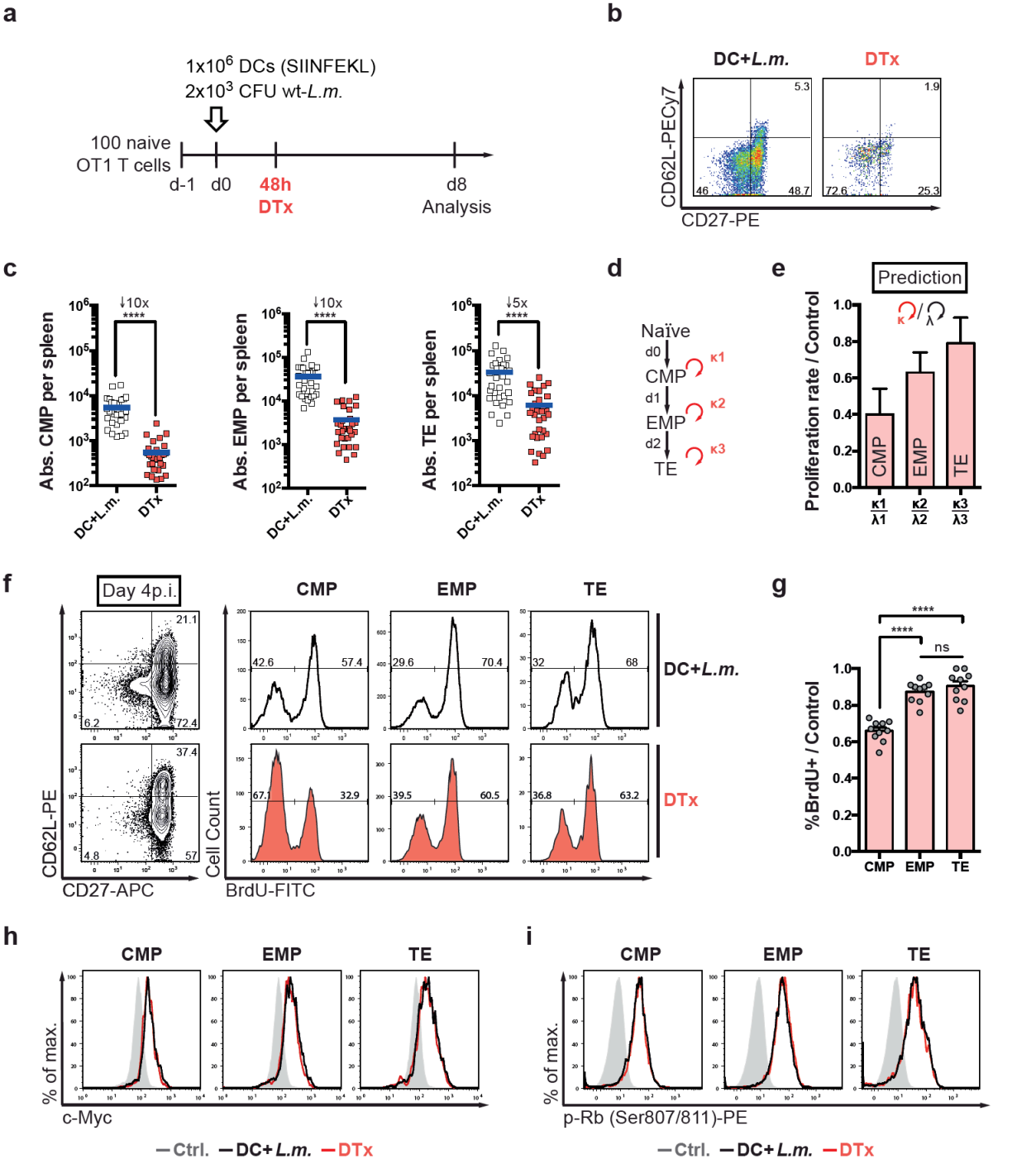

Figure 9 | Depletion of antigenic stimuli leads to a pronounced delay in cell cycle progression of CMPs. a. Scheme of the experimental setup and DC depletion strategy. **b-c.** Progenies were recovered from spleen per transferred 100 OT1 cells at day 8 after immunization (n=30), as well as following DTx treatment at 48h (n=32). **b.** Representative pseudo-color plots showing expression of CD62L and CD27 for transferred T cells. **c.** Scatter plots depict absolute numbers of CMP, EMP and TE cells. **d.** Adjusted model used for fitting to the experimental data, characterized by altered proliferation rates (κ_1–κ_3), effective 12h after DTx treatment. **e.** Bar graph depicts predicted proliferation rates, relative to those of the untreated control group. **f-g.** BrdU labelling was performed as in Figure 6e, but with DTx treatment at 48h. **f.** Representative contour plots showing expression of CD62L and CD27 on transferred T cells, with corresponding histograms showing the BrdU profiles for the indicated subsets. **g.** Bar graph depicts the percentage of $BrdU^+$ cells relative to the mean of the untreated control group (n=10). **h-i.** Representative histograms show expression of (**h**) c-Myc and (**i**) retinoblastoma protein (Rb) phosphorylated at Ser807/811 (grey: endogenous naïve $CD8^+$ T cells) for transferred OT1 cells at day 4p.i. Lines indicate the mean, error bars the s.e.m. ****$P < 0.0001$ (Mann-Whitney test). Data are from four (**b, c**), two (**f, g**) or one of two independent experiments (**h, i**) (modified from Kretschmer et al., 2020).

markers were previously reported to become undetectable within minutes, after ubiquitin-mediated proteolysis (Kim et al., 2003) or hypo-phosphorylation upon cell cycle exit (Moser et al., 2018), respectively. Finally, cells from all subsets displayed blastoid morphology, both in presence or absence of antigenic stimuli (Figure 10). Taken together, these results demonstrate that DC depletion lead to a pronounced delay of the CMP cell cycle, without inducing any immediate division-cessation.

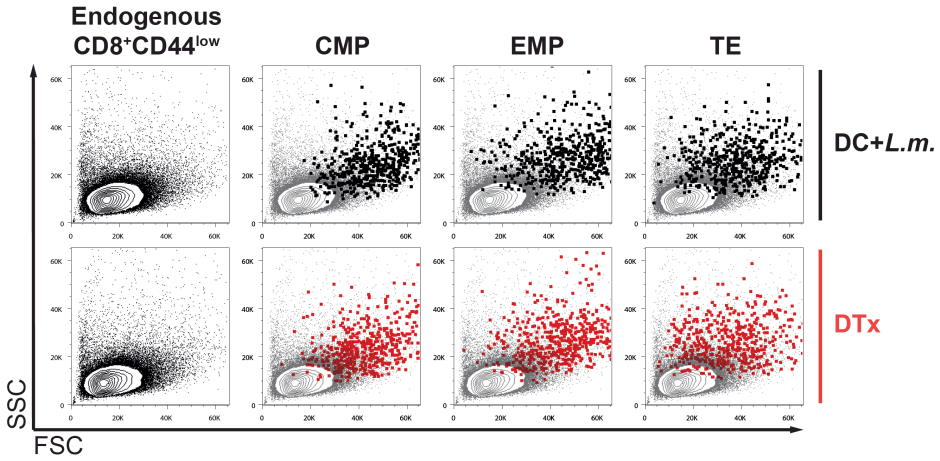

Figure 10 | T cell blast size is not affected by depletion of antigen-presenting DCs. C57BL/6 mice received adoptive transfer of 10.000 naïve OT1 cells and, one day later, were immunized with DC+*L.m.* Representative contour plots showing the Forward- (FSC) / Side Scatter (SSC) profiles for progenies recovered from spleen at day 4 after DC+*L.m.* immunization (black dots), as well as following DTx treatment at 48 hours (red dots), shown against the background of the endogenous naïve $CD8^+$ T cell compartment within the same recipients (left, and grey background) (modified from Kretschmer et al., 2020).

4.4. Measuring the speed of cell cycle progression *in vivo*

Having established that differences in cell cycle regulation indeed accompanied the differentiation step from CMP to non-CMP cells *in vivo*, raised the question of which cell cycle phases contributed to this process. Traditionally, this can be addressed by measuring the total cellular DNA-content, varying between diploid (DNA^{2N}) to tetraploid (DNA^{4N}) in dividing cells, with concomitant BrdU detection after short pulse durations of around 0.5 hours (Dowling et al., 2014). Thereby, cells located in G1 ($BrdU^-DNA^{2N}$) can be distinguished from cells in S phase ($BrdU^+DNA^{2\text{-}4N}$), and G2M ($BrdU^-DNA^{4N}$) (Figure 11a).

First, applying this strategy for CD62L$^+$ CMPs and CD62L$^-$ non-CMPs after DC+*L.m.* immunization as well as DTx treatment revealed substantial inter-subset differences in G1 and S phase distribution at day four (Figure 11b and c): CMPs thus showed relatively more cells localized in G1 and fewer cells in S phase, compared to non-CMPs, under both experimental conditions. Interestingly, these differences in cell cycle distribution were, however, clearly enhanced after depletion of antigenic stimuli. Conversely, the fraction of cells in G2M was low and remained virtually unchanged by DC depletion (Figure 11b and c). While these experiments highlighted the relative contributions of the G1, S, and G2M phases in establishing the proliferation speeds of CMPs and non-CMPs, their absolute cell cycle phase lengths (i.e. durations), so far, remained uncertain.

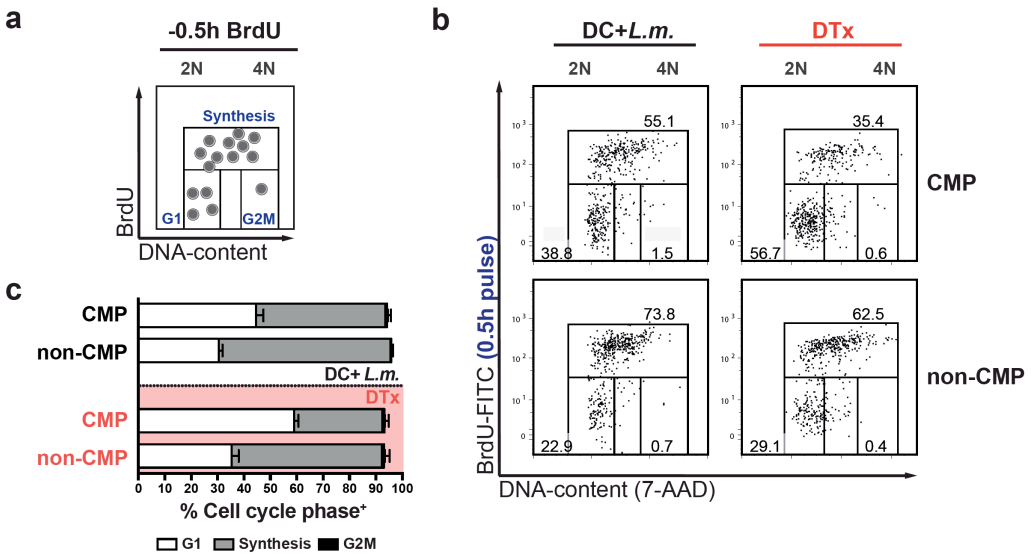

Figure 11 | Differences in cell cycle distribution between CMPs and non-CMPs are enhanced upon DC depletion. a. Schematic representation of cells distributed throughout all active phases of the cell cycle in BrdU/DNA plots. **b-c.** Experiments were performed as in Figure 9f, but BrdU incorporation and 7-AAD staining of DNA-content were analyzed 0.5h after BrdU injection. **b.** Representative dot plots showing BrdU/DNA profiles of CD62L$^+$ (CMP) and CD62L$^-$ (non-CMP) cells derived from transferred T cells at day 4 after immunization (DC+*L.m.*), as well as after DTx treatment (DTx). **c.** Bar graph depicts the percentage of cells in the indicated cell cycle phases (DC+*L.m.* and DTx, n=4). Lines indicate the mean, error bars the s.e.m. Data are from two independent experiments (modified from Kretschmer et al., 2020).

In order to overcome this limitation in our setup, the duration of the overall cell cycle needed to be reliably quantified. Such an approach was developed in close collaboration with the computational modeling group of Dr. Michael Flossdorf (Technische Universität München,

Germany) and is based on experimentally measuring the fraction of cells that divide within a given time frame *in vivo*: in principle, T cells that were labelled with BrdU during S phase, but have divided before their DNA-content was analyzed should become detectable as $BrdU^{+}DNA^{2N}$ (Figure 12a, blue cells). Using this fraction of $BrdU^{+}DNA^{2N}$ cells, together with the previously determined G2M-fraction, already suffices to determine the average duration of the overall cell cycle in a straightforward mathematical calculus (Figure 12b).

For short pulse durations of 0.5 hours, the $BrdU^{+}DNA^{2N}$ population can, however, also contain cells that have freshly entered S phase towards the tail end of the labelling period (Figure 12a, left: red cells). We speculated that a better separation of these early S phase cells from the $BrdU^{+}DNA^{2N}$ divided-cell population should be obtained by extending the time lag between injecting BrdU and analyzing DNA-content to 3.0 hours (Figure 12a, right). This delay builds on the assumption that the bioavailability of BrdU, when administered as a single i.p. dose to mice, rapidly decreases after 15 minutes *in vivo* (Matiašová et al., 2014) and would thus prevent early S phase cells from localizing into the $BrdU^{+}DNA^{2N}$ compartment (Figure 12a, right: red cells).

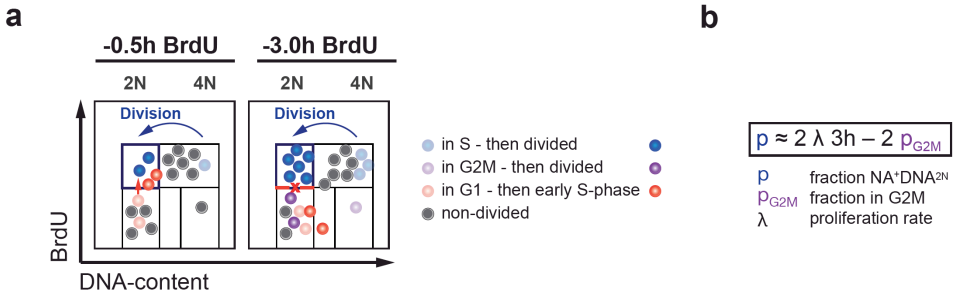

Figure 12 | Cell cycle progression after BrdU-pulsing can be used to discriminate T cells that divide within the observation period. a. Schematic representation of cell cycle progression in BrdU/DNA plots, for cells located in different cell cycle phases at the time of BrdU injection, as indicated (right). **b.** The mathematical formula to calculate the division rate λ from the fraction of cells in G2M and the $BrdU^{+}DNA^{2N}$ gate is given for BrdU injection 3.0 hours before analysis (right, upper panel). This approach was developed in collaboration with the laboratory of Dr. Michael Flossdorf (Technische Universität München, Germany) (modified from Kretschmer et al., 2020).

To first confirm these assumptions, BrdU incorporation was analyzed either 0.5 or 3.0 hours after injection. Remarkably, no difference could be found between both conditions, suggesting that no relevant BrdU uptake had occurred beyond 0.5 hours of injection (Figure 13a and b). Next, it was tested whether our approach would provide an accurate temporal resolution of cell cycle

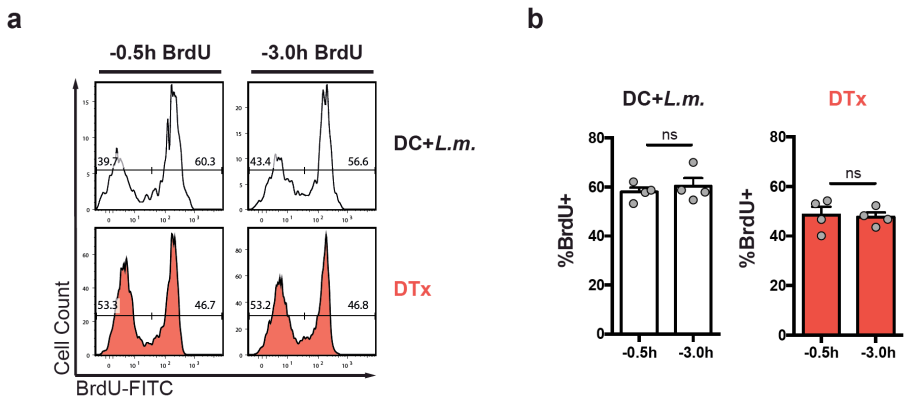

Figure 13 | No relevant label uptake occurs beyond 0.5 hours after BrdU-pulsing. Progenies were recovered from spleen per transferred 10^4 naïve OT1 cells at day 4 after DC+*L.m.* immunization, as well as following DTx treatment at 48h. BrdU was injected either 0.5 or 3.0 hours before analysis, respectively. **a.** Representative histograms showing the BrdU profiles for transferred T cells. **b.** Corresponding bar graphs depict the percentage of $BrdU^+$ cells in the indicated experimental groups (n=4). Lines indicate the mean, error bars the s.e.m. (Mann-Whitney test). Data are from two independent experiments (modified from Kretschmer et al., 2020).

progression. To this end, a double-labelling strategy was devised, in which the nucleoside analogues EdU and/or BrdU were administered 3.0 and 0.5 hours before analysis, respectively (Figure 14). Importantly, no cross-reactivity in the detection of these labels was observed, as evidenced by the EdU/BrdU profiles of mice that had been injected with either EdU or BrdU alone (Figure 14 a and b). According to the default temporal spacing of the EdU and BrdU label injections, the fraction of S phase cells that subsequently divided within the 3.0 hour observation period (EdU^+DNA^{2N}) should be composed of roughly 5/6 $BrdU^-$ and 1/6 $BrdU^+$ cells (Figure 14c). Indeed, analyzing the fraction of EdU^+DNA^{2N} cells that had also incorporated BrdU provided an accurate measure for these estimates (Figure 14d). This confirmed that our measurements of divided T cells in the EdU^+DNA^{2N}-gate indeed captured the temporal differences, introduced by the particular spacing of the sequential EdU und BrdU injections in this experiment.

When subsequently investigating the DNA/BrdU profiles of CMPs and non-CMPs responding to DC+*L.m.* immunization, it became apparent that CMPs contained fewer $BrdU^+DNA^{2N}$ cells than non-CMPs after the 3.0 hour pulsing period (Figure 15a, left). Intriguingly, this difference was further enhanced upon depletion of antigenic stimuli, coinciding with a pronounced reduction of $BrdU^+DNA^{2N}$ cells in the CMP compartment (Figure 15a, right). Using these measurements and the previously determined G2M fraction of cells (Figure 11), which also divide during the

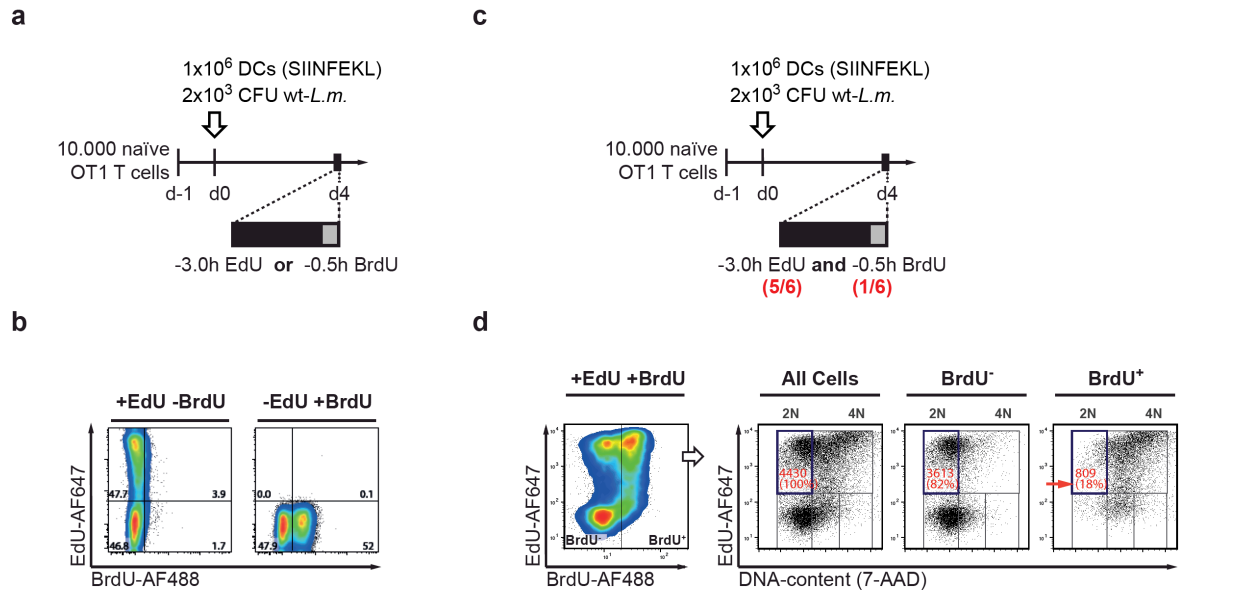

Figure 14 | Validating the temporal resolution of cell cycle speed measurements. a. Scheme of the experimental setup using either EdU or BrdU labelling, 3.0 or 0.5h before analysis, respectively. **b.** Representative pseudo-color plots showing the EdU/BrdU profiles for transferred T cells. **c.** As in **a.**, but using sequential EdU and BrdU double-labelling. **d.** Representative pseudo-color plot showing the EdU/BrdU profile for transferred T cells and corresponding dot plots showing EdU against total cellular DNA-content for all cells, or pre-gated on $BrdU^-$, and $BrdU^+$ cells. Numbers indicate the amount of cells located in the EdU^+DNA^{2N} gate (Divided cells) and numbers in parenthesis the percentage among all measured EdU^+DNA^{2N} cells (All cells). Data are representative of two independent experiments (modified from Kretschmer et al., 2020).

observation period despite remaining $BrdU^-$, allowed to quantify the average durations of the overall cell cycle, but also that of its constituting phases (Figure 15b). These calculations, carried out by our collaboration partners, revealed that CMPs and non-CMPs needed an average of 8.6 and 6.2 hours to complete their cell cycle in the presence of antigen-presenting DCs, respectively (Figure 15b, „DC+*L.m.*). Following depletion of antigenic stimuli, CMPs markedly elongated their cell cycle and divided only once every 17.0 hours, opposed to non-CMPs, which could better maintain their faster inter-division speeds and divided every 9.7 hours (Figure 15b, „DTx“). Intriguingly, the different cell cycle durations of CMPs and non-CMPs resulted almost exclusively from differences in their G1 phases. Upon DC depletion, these differences in G1 further increased, but also coincided with an elongation of S phase in both subsets (Figure 15b).

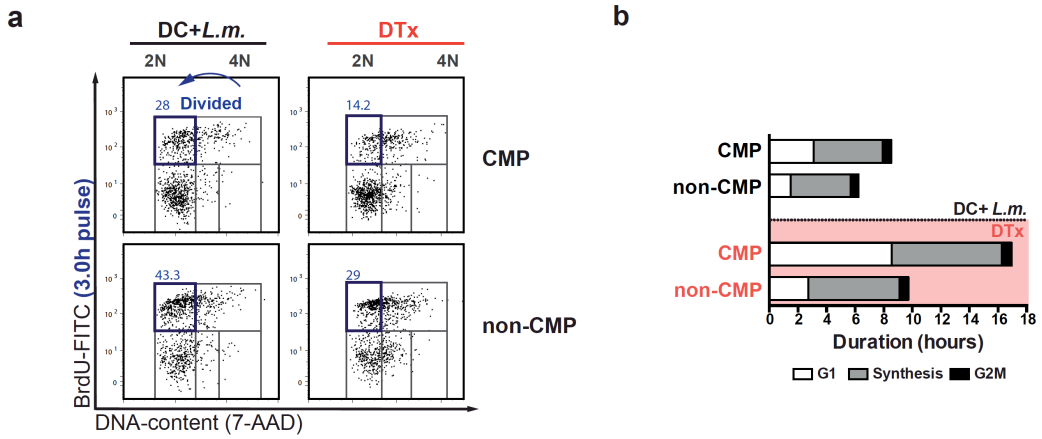

Figure 15 | Cell cycle speed of CMPs and non-CMPs is differentially regulated by elongation of G1 and S phase. a-b. Experiments were performed as in Figure 9f, but BrdU incorporation and 7-AAD staining of DNA-content were analyzed 3.0h after BrdU injection. **a.** Representative dot plots showing BrdU/DNA profiles of CD62L$^+$ (CMP) and CD62L$^-$ (non-CMP) cells derived from transferred T cells at day 4 after immunization (DC+*L.m.*), as well as after DTx treatment (DTx). **b.** Bar graph depicts the calculated average division times with respective cell cycle phase lengths for the indicated subsets among transferred T cells. This result was obtained in collaboration with the laboratory of Dr. Michael Flossdorf (Technische Universität München, Germany). Lines indicate the mean, error bars the s.e.m. Data are from two independent experiments (modified from Kretschmer et al., 2020).

4.5. DNA replication during S phase is delayed in absence of antigenic stimuli

The experiments outlined above suggested that changes in cell cycle speed within expanding CD8$^+$ T cell populations also encompassed a regulation of the S phase length. Recently, elegant approaches based on sequential EdU and BrdU labelling have revealed that CD4$^+$ T cell help accelerates the speed of DNA replication during S phase in germinal center B cells (Gitlin et al., 2015). In this setup, it was shown that cells can be assigned to their respective position in S phase according to their individual EdU/BrdU profiles, thereby distinguishing early S phase (EdU$^-$BrdU$^+$), mid/late S phase (EdU$^{low/high}$BrdU$^+$), post S phase (EdU$^+$BrdU$^-$), and G1 (EdU$^-$BrdU$^-$) cells (Gitlin et al., 2015; Gitlin et al., 2014).

Based on these findings, a similar EdU/BrdU-labelling strategy was adopted to investigate S phase progression of CD8$^+$ T cells cycling in presence or absence of antigen. To this end, EdU and BrdU were injected 3.0 and 0.5 hours before analysis at day 4 after DC+*L.m.* immunization, respectively (Figure 16a). DNA-content measurements in different EdU/BrdU-subpopulations initially confirmed that the previously described allocation to distinct cell cycle phases correlated with an increase in DNA replication during S phase progression (Figure 16b). In contrast, post S phase cells showed DNA profiles similar to that of G1, indicating that division had occurred.

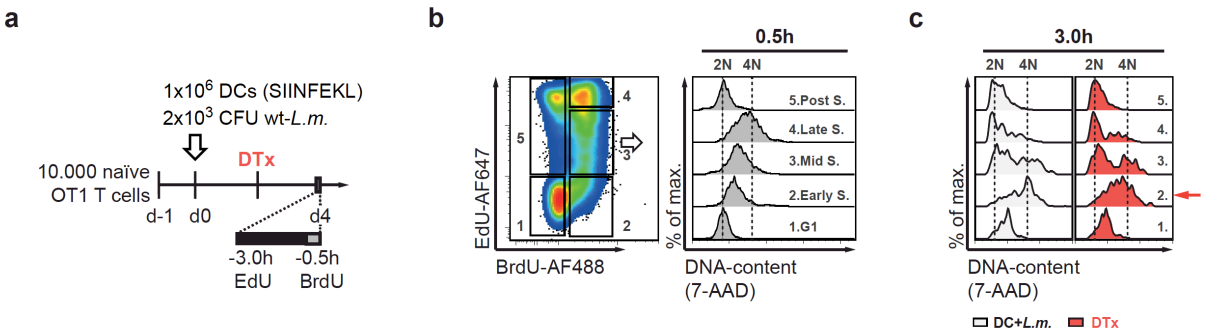

Figure 16 | DNA replication during S phase is delayed in absence of antigenic stimuli. a. Scheme of the experimental setup used to track S phase progression by sequential EdU and BrdU labelling. **b.** Representative pseudo-color plot showing the EdU/BrdU profile of transferred T cells with corresponding overlayed histograms showing the DNA-content for the indicated EdU/BrdU-subpopulations (1-5); DNA labelling 0.5h after BrdU pulse. **c.** Representative overlayed histograms showing the DNA-content for the same subpopulations; DNA labelling 3.0h after BrdU pulse. Data are representative for one of two independent experiments (modified from Kretschmer et al., 2020).

By extending the time lag between administering BrdU and DNA-content analysis to 3.0 hours, it became clear that DNA-content had changed within the previously defined EdU/BrdU subpopulations, as cells continued to cycle in absence of continued BrdU labelling (Figure 16c). Importantly, cells that previously localized in early S phase (~DNA^{2N}) during BrdU-pulsing had undergone considerable DNA synthesis during the follow up time frame in the untreated vaccination group (Figure 16c, lane 2: „DC+*L.m.*“). In contrast, this increase in DNA-content was not as strongly pronounced for cells that were cycling in the absence of antigenic stimuli, indicating that DNA replication was delayed (Figure 16c, lane 2: red arrow, „DTx“). Remarkably, cells that were initially assigned to G1 phase had clearly entered S phase under both antigen replete and depleted conditions ($DNA^{>2N}$) (Figure 16c, lane 1: „DC+*L.m.* and DTx“), thus further confirming our previous findings that cell cycle exit to G0 had not occurred. By using the enhanced resolution provided by combinatorial EdU and BrdU-pulsing, with DNA-content measurements, these experiments collectively demonstrated that sustained antigenic stimuli supported the faster DNA-replication in $CD8^+$ T cells during S phase transition of their cell cycle.

4.6. Inflammatory stimuli support faster cycling of effector T cell subsets

The observation that CMPs and non-CMPs were differentially affected by depletion of antigen-presenting DCs, raised the question of whether the faster cell cycles of non-CMPs were instead

maintained by TCR-independent growth signals. Inflammatory cytokines have been previously implicated in prolonging the division program of activated CD8$^+$ T cell populations *in vitro* and *in vivo*, by inducing up-regulation of the high-affinity IL-2 receptor α-chain (CD25) (Kaech et al., 2001; Starbeck-Miller et al., 2014). On the one hand, sustained expression of CD25 promotes the transcriptional program of TEs and thus drives terminal differentiation (Pipkin et al., 2010). On the other hand, enhanced IL-2 signaling has been shown to accelerate the G1 to S phase transition via the PI3K-E2F pathway (Brennan et al., 1997) and could thereby also represent a potential modulator of cell cycle speed.

To explore a potential contribution of IL-2 signaling in regulating the distinct cell cycle activities of CMPs and non-CMPs during DC+*L.m.* vaccination, expression levels of CD25 were assessed at day four and found to be inversely correlated with the expression of CD62L (Figure 17a). These differences were indicative of IL-2 responsiveness, as only CD25^{high} cells induced strong

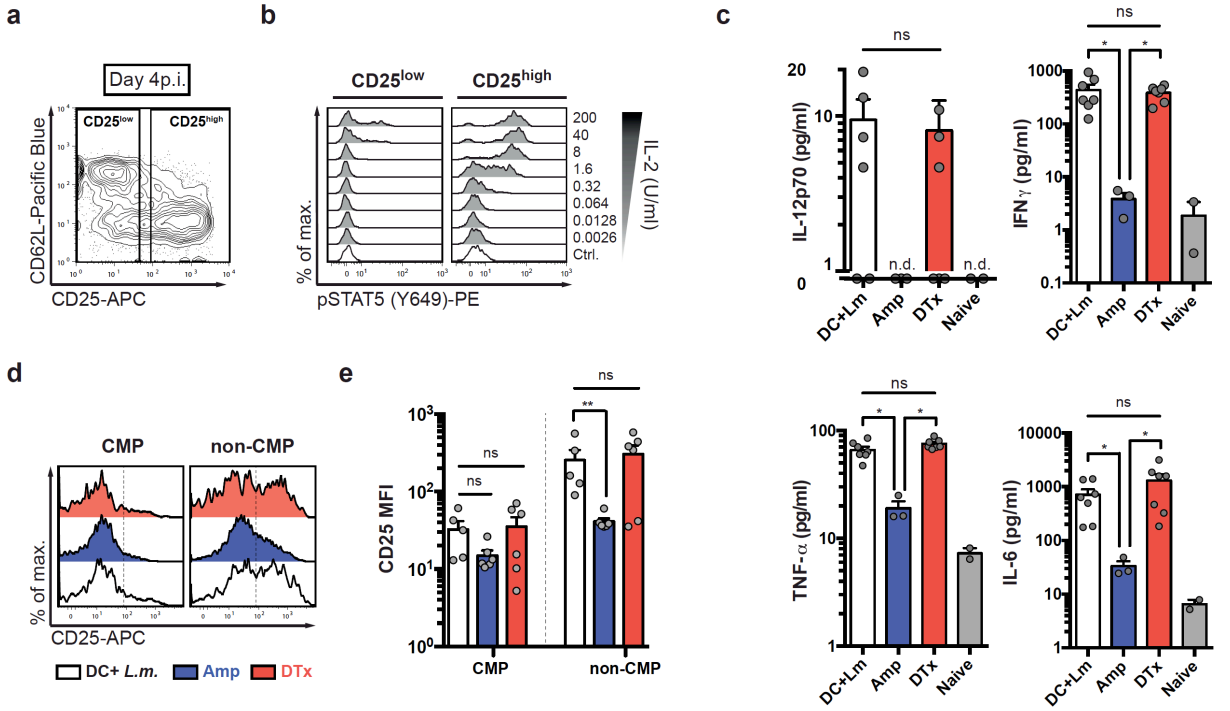

Figure 17 | Inflammatory cytokines, but not sustained antigenic stimuli confer enhanced IL-2 responsiveness to non-CMPs via up-regulation of CD25. a. Representative contour plot showing expression of CD62L and CD25 for progenies derived from 10^4 naïve OT1 cells at day 4 after DC+*L.m.* immunization. **b.** As in **a.**, but splenocytes were re-stimulated *ex vivo* with titrated amounts of IL-2 for 15min. Overlayed histograms showing pSTAT5 (Y649) for CD25^{low} and CD25^{high} subsets of transferred OT1 cells. **c.** C57BL/6 mice were immunized with DC+*L.m.* and either left untreated (n=7) or received Amp (n=3) or DTx (n=7) treatment. Cytokine measurements were performed at 2.5 days after immunization. **d.** As in **a.**, but mice were either left untreated (DC+*L.m.*; n=5) or received Amp (n=6) or DTx (n=6) treatment. Histograms showing expression of CD25 for the indicated subsets. **e.** Bar graph depicts the CD25 median fluorescent intensity (MFI) values. Lines depict the mean, error bars the s.e.m. $*P < 0.05$, $**P < 0.01$ (Mann-Whitney test). Data are from two independent experiments (modified from Kretschmer et al., 2020).

STAT5 phosphorylation upon *ex vivo* re-stimulation, whereas $CD25^{low}$ cells failed to respond even to higher doses of IL-2 (Figure 17b).

Initially, expression of CD25 can be induced by antigenic stimulation perceived during priming, but is then quickly lost by most cells as they begin to proliferate. At later time points, inflammatory cytokines, such as IL-12, are thought to sustain CD25 expression on a fraction of proliferating cells. Interestingly, it has been shown that priming DCs are, however, not the relevant source of IL-12 in different DC vaccination approaches, but that bystander DCs and macrophages of the host instead supply this critical cytokine (Cui et al., 2009).

Following this assumption, sustained CD25 expression by activated $CD8^+$ T cells during DC+*L.m.* immunization should not depend on the continued presence of antigen-presenting DCs, but rather on the inflammatory milieu induced by the background *L.m.*-infection. When monitoring serum levels of IL-12, IFN-γ, TNF-α, and IL-6 in the unperturbed DC+*L.m.* as well as the DTx-treated setting, it became clear that DC depletion did in fact not influence the systemic concentration of these cytokines (Figure 17c). However, by curtailing *L.m.*-infection after administration of the antibiotic ampicillin (Amp), a severe decline could be detected for all cytokines (Figure 17c). Importantly, this decline critically coincided with a pronounced reduction in CD25 expression of non-CMPs after Amp treatment, compared to the DC+*L.m.* and DTx-treated groups (Figure 17d and e). In contrast, CD25 expression by CMPs was substantially lower than for non-CMPs and was not affected by either Amp or DTx administration.

Building on these distinct CD25 expression patterns between CMPs and non-CMPs, an adoptive co-transfer system was devised to directly compare the proliferative capacities of OT1 CD25 knockout (KO) and OT1 CD25 wild type cells under identical experimental conditions. At day four after DC+*L.m.* immunization, both CD25-KO and CD25-wt OT1 cells could be segregated according to their congenic phenotypes (Figure 18a, left). As expected, CD25-KO OT1 cells completely lacked expression of CD25 (Figure 18a, right), but also showed a remarkable increase in the percentage of CMP cells (Figure 18a and b). To test, whether this relative increase in CMPs had resulted from an impaired proliferation capacity of non-CMP cells, BrdU uptake was assessed in both subsets after 3.0 hours of labelling. While no difference were found for CMPs between the CD25-KO and CD25-wt populations, non-CMPs indeed showed a significant reduction in percentage of $BrdU^+$ cells when CD25 was lacking (Figure 18c and d). Notably, the difference in BrdU uptake between CMPs and non-CMPs of the CD25-KO population were not

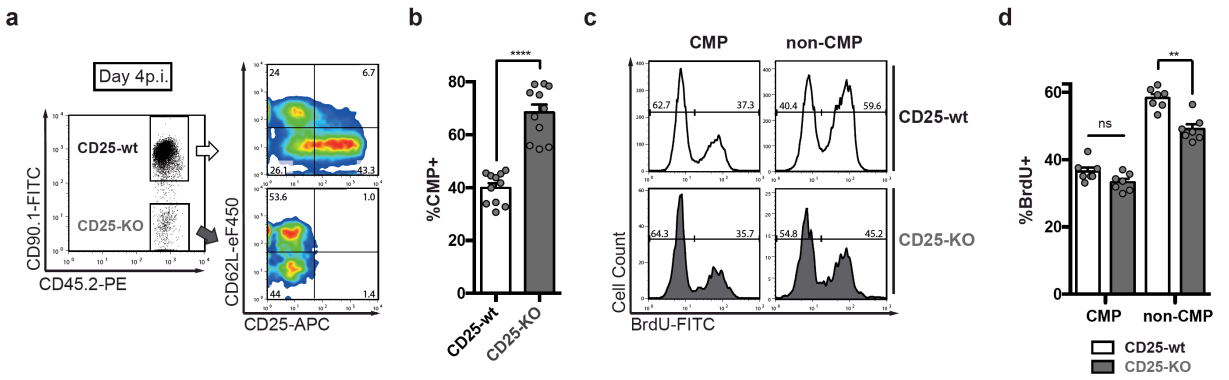

Figure 18 | Enhanced IL-2 responsiveness supports faster proliferation of non-CMPs. 5x10^4 naïve CD25-wt (CD45.1$^{-/-}$CD90.1$^{+/+}$) and 5x10^4 naïve CD25-KO (CD45.1$^{-/-}$CD90.1$^{-/-}$) OT1 cells were transferred into CD45.1$^{+/+}$CD90.1$^{-/-}$ recipients, followed by DC+*L.m.* immunization. BrdU was injected 3h before analysis. **a.** Representative dot plot showing the gating strategy for transferred OT1 cells (pre-gated: CD8$^+$CD45.2$^+$CD45.1$^-$), with corresponding pseudo-color plots showing expression of CD62L and CD25. **b.** Bar graph depicts the percentage of CMP cells (n=11). **c.** Representative histograms showing the BrdU profiles of the indicated subsets. **d.** Bar graph depicts the percentage of BrdU$^+$ cells (n=7). Lines depict the mean, error bars the s.e.m. $^{**}P < 0.01$, $^{****}P < 0.0001$ (Mann-Whitney test) (modified from Kretschmer et al., 2020).

completely abolished, suggesting that additional cell-intrinsic or extrinsic factors might have additional roles in establishing this subset-specific effect.

Collectively, these results indicate that the faster cell cycles of non-CMPs were reinforced by inflammatory cytokines, through enhanced CD25-mediated high-affinity IL-2 signaling. The fact that CMPs apparently lacked this ability might, in turn, leave them more dependent on sustained antigenic stimulation.

4.7. Distinct effects of antigen and inflammation on memory CD8$^+$ T cell development

In light of the distinctly regulated cell cycle activities of CMPs and non-CMPs, the long-term memory potential of CD8$^+$ T cells, developing in absence of either antigenic or inflammatory stimuli needed to be investigated (Figure 19a). Interestingly, when monitoring immune responses generated from 100 naïve OT1 cells in peripheral blood at day eight, both DTx and Amp treatment equally reduced the response magnitude, compared to the untreated DC+*L.m.* control group (Figure 19b and c). However, when subsequently challenging mice with a recombinant *L.m.*-OVA infection, memory T cell responses in the Amp-treated group were similarly strong as

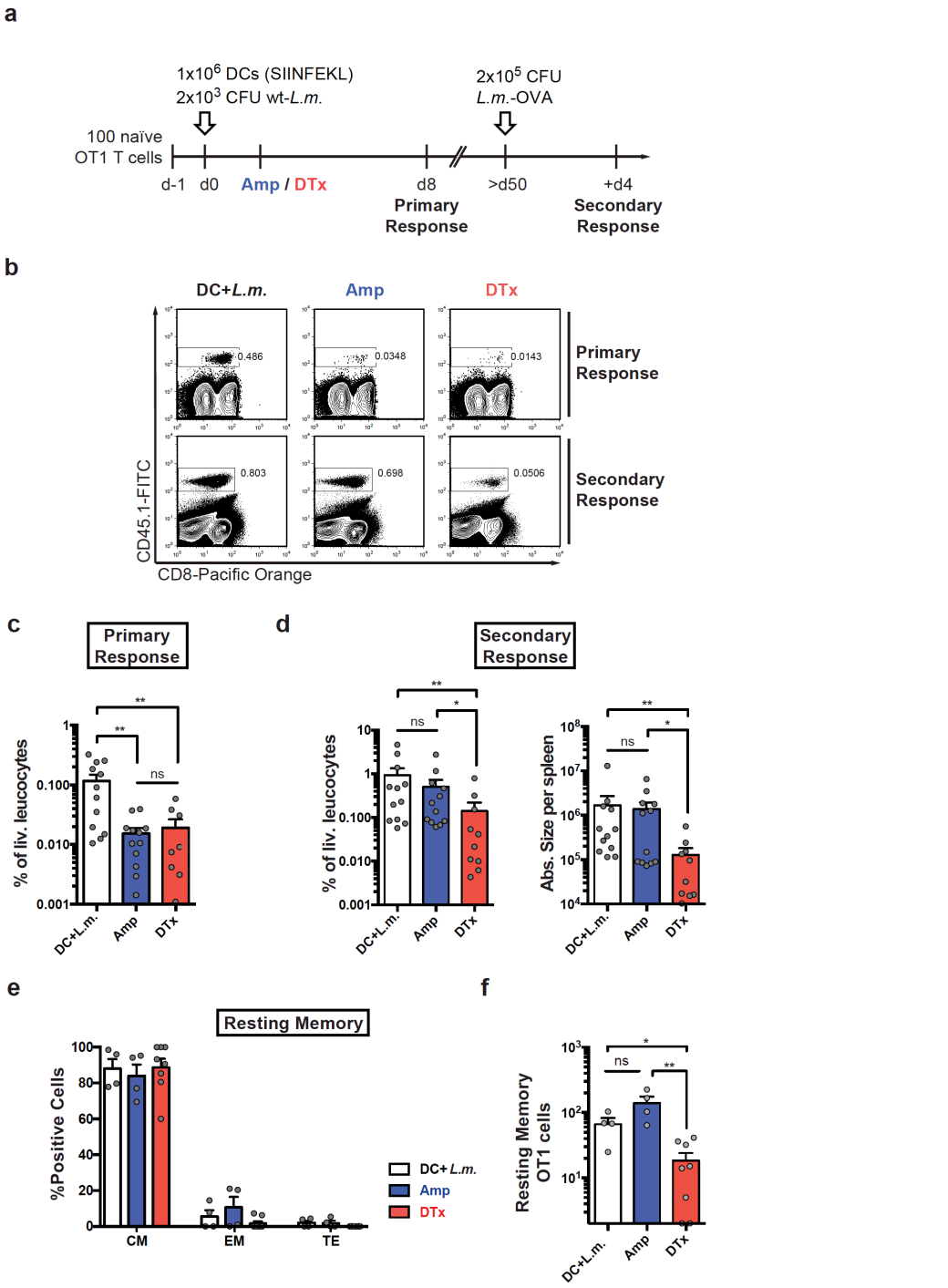

Figure 19 | Sustained antigen availability during priming, but not inflammation supports strong memory CD8⁺ T cell responses. a. C57BL/6 mice received 100 naïve OT1 cells and were immunized with DC+*L.m.* Mice then either received Amp at 24h (n=12), DTx at 48h (n=10), or were left untreated (DC+*L.m.*; n=10). Progeny were screened in peripheral blood at day 8 and then longitudinally analyzed 4 days after a re-challenge infection with recombinant *L.m.*-OVA. **b.** Representative contour plots showing the percentage of transferred T cells among living leucocytes during the primary (upper row) and secondary immune response (lower row). **c.** Bar graph depicts the percentage of transferred T cells among living leucocytes at day 8 (DTx: n=2 progenies initially not detected). **d.** Bar graphs depict the percentage of transferred T cells among living leucocytes (left) and absolute number of daughter cells in spleen (right) at day 4 after *L.m.*-OVA re-challenge. **e.** Bar graph indicates the percentage of resting memory T cells (no re-challenge) of central memory (CM), effector memory (EM) or TE phenotype, at 6 weeks post immunization (DC+*L.m.*, n=4; Amp, n=4; DTx, n=8). **f.** Bar graph indicates corresponding numbers of resting memory T cells in spleen and lymph nodes. Lines depict the mean, error bars the s.em. $*P < 0.05$, $**P < 0.01$ (Mann-Whitney test). Data are from two independent experiments (modified from Kretschmer et al., 2020).

those generated in the untreated vaccination group (Figure 19d). In contrast, premature depletion of antigen-presenting DCs during primary expansion coincided with a ~10-fold reduction in memory T cell responses (Figure 19d).

In order to explore whether these distinct recall capacities emerged from preceding changes within the resting memory T cell compartment, absolute memory OT1 cell numbers, as well as their phenotypic composition were analyzed in absence of secondary stimulation. Interestingly, most memory T cells recovered from spleen and lymph nodes six weeks after primary immunization displayed a clear CM phenotype, and only very little effector memory EM or TE cells could be found (Figure 19e). However, significantly fewer numbers of resting memory OT1 cells were detectable following initial DTx treatment, compared to both the Amp as well as untreated DC+*L.m.* vaccination group (Figure 19f).

These findings highlight that the sustained availability of antigen, but not inflammatory cues, critically regulates the cell cycle speed of CMPs throughout primary expansion, and is thereby highly beneficial for expanding a stronger memory $CD8^+$ T cell compartment.

5. Discussion

5.1. Clonal expansion of CD8$^+$ T cell subsets is regulated by division speed

Naïve CD8$^+$ T cells are characterized by an outstanding capacity to proliferate in response to antigenic stimulation (Zhang et al., 2011). During the first week of infection or vaccination, antigen-specific T cells are estimated to complete as many as 15-20 rounds of cell division, thereby increasing their population size by several orders of magnitude (Lanzavecchia et al., 2000; Williams et al., 2007). This expanded CD8$^+$ T cell population is eventually dominated by armed-effector T cells, mediating acute pathogen clearance, compared to a much smaller population of memory precursors, providing long-term immunity to re-infection (Badovinac et al., 2006; Buchholz et al., 2016; Kaech et al., 2012). Deciphering the developmental pathways of distinct CD8$^+$ T cell subsets has remained a long-standing goal in immunology and carries important implications for vaccine development (Kaech et al., 2002; Williams et al., 2007) as well as adoptive T cell therapy (Busch et al., 2016; Klebanoff et al., 2012).

In this work, we applied single CD8$^+$ T cell fate mapping and novel approaches for *in vivo* cell cycle analysis to better resolve the proliferation and differentiation dynamics of emerging T cell subsets. We thereby identified a crucial proliferative hierarchy that separates slowly cycling CMPs from more rapidly proliferating EMPs, and TEs during the early stages of a CD8$^+$ T cell response. A key feature of this finding lies in the subset-specific regulation of clonal expansion via distinct cell cycle speeds. This concept challenges previous *in vitro* studies that have proposed rather homogenous inter-division times for activated CD8$^+$ T cells (Gett et al., 2000; Marchingo et al., 2014), followed by a differential cessation of division activity, depending on the nature and strength of initial stimulation (Heinzel et al., 2017; Marchingo et al., 2016). Importantly, we found no evidence for such premature division cessation beyond the first six days of T cell proliferation *in vivo*, however, our results do not rule out a differential timing of cell cycle dropout in CMPs and their more terminal (non-CMP) effector descendants at later time points. In fact, it has been described that mitogenic stimuli, such as antigen and/or inflammation, persist throughout the larger parts of the expansion phase and only begin to subside around the peak of the pathogen-specific CD8$^+$ T cell response (Cockburn et al., 2010; Kim et al., 2010; van

Faassen et al., 2004; Zammit et al., 2006). These findings therefore argue that the programmed division cessation, described *in vitro*, might become increasingly more relevant during the later stages of primary immune responses *in vivo*.

Further on, it should be considered that the subset-specific cell cycle speeds, identified in this study, can only translate into distinct outputs of CMPs and non-CMPs, if both subsets cease to proliferate at somewhat similar time points. In response to DC+*L.m.* vaccination, all responding T cells remained in the cell cycle throughout most of the expansion phase. However, already by day four, CMPs divided more slowly than their more-terminal effector counterparts.

These findings appear to contradict previous reports that have proposed a substantial divergence in the cell-cycle activities of MPs and TEs only towards the later stages of clonal expansion (Kinjyo et al., 2015; Sarkar et al., 2008). Indeed, our measured differences in the inter-division times of CMPs (8.6 hours) and non-CMPs (6.2 hours) at day four may initially appear small. However, these measurements define proliferation rates of roughly 3 and 4 cell divisions per day, for CMPs and non-CMPs, respectively. In absence of premature division cessation, leading up to the peak of the response at day eight, these estimates will eventually translate into a 2^{12}-fold expansion (2^{3x4}) of the CMP- and 2^{16}-fold (2^{4x4}) expansion of the non-CMP compartment. Thus, within a four-day period of continued proliferation, non-CMPs should achieve a striking 16-fold ($2^{16} : 2^{12} = 2^4$) outgrowth over CMPs. These extrapolations fit surprisingly well to the measured fractions of ~5-10% CMPs and 90-95% non-CMPs within an expanded $CD8^+$ T cell population, at the peak of a primary immune response. They thereby highlight how small differences in cell cycle speed between emerging immune cell subsets can suffice to mediate drastically distinct proliferative outcomes. Such differences could previously not be resolved by traditional NA-labelling approaches (Sarkar et al., 2008), lacking the necessary temporal resolution of cell cycle progression, or were considered negligible in *ex vivo* live-cell imaging studies (Kinjyo et al., 2015).

5.2. Reciprocal regulation of cellular differentiation and division speed

Our quantification of key cell cycle parameters in CMPs and non-CMPs could further open up new perspectives on the coordinate regulation of division speed and cellular differentiation in activated $CD8^+$ T cells. A potential coupling of these fundamental processes has been previously

suggested in various mathematical models of T cell diversification (Buchholz et al., 2013a; Cho et al., 2017; Schlub et al., 2009). However, it has so far remained exceedingly difficult to experimentally quantitate either parameter in an *in vivo* setting.

Traditional dye-dilution techniques (e.g. CFSE-labelling) (Yoon et al., 2010) are limited to visualizing the first 7-8 cell divisions after initial T cell activation and can only reveal the net outcome of differentiation and proliferation events over a multi-day observation period. This approach is not suitable for disentangling the highly dynamic proliferation and differentiation processes that unfold in parallel during the early stages of T cell proliferation and can not be used at later time points, when the division-dye is fully diluted. FUCCI-reporter systems (Kinjyo et al., 2015; Sakaue-Sawano et al., 2008) or measurements of NA uptake (e.g. BrdU/EdU) and DNA-content (Nunez, 2001) can resolve the current position of dividing $CD8^+$ T cells within the cell cycle, but can not be used to determine their speed of cell cycle progression. The methodology presented in this work overcame this limitation. It explicitly relied on delaying DNA analysis from 0.5 to 3.0 hours after NA-pulsing, which allowed NA^+ T cells to complete their S phase and undergo mitosis, as indicated by a partitioning of DNA-content to newly generated daughter cells. By experimentally measuring this fraction of cells that divided within a given NA-observation period for CMPs and non-CMPs, the cell cycle speed of these subsets could be accurately determined. Our analyses thereby confirm central model predictions, derived from *in vivo* single cell fate mapping experiments, proposing a differentiation-dependent increase of cell cycle speed upon transition from CMPs into non-CMPs (Buchholz et al., 2013a).

In addition, we establish that the differences in division speed between emerging $CD8^+$ T cell subsets originated mainly from variations in G1 length, rather than an overall stretching of all underlying cell cycle phases, as previously suggested (Dowling et al., 2014).

The measured inter-division times of CMPs and non-CMPs (8.6 - 6.2 hours) in presence of antigen, moreover, appear exceedingly fast. In comparison, it is currently estimated that mouse embryonic stem cells and inducible pluripotent stem cells adopt one of the fastest mammalian cell cycles, amounting to ~12 hours (Guo et al., 2014). In these *"ultra-rapid"* cell types, a pronounced truncation of G1 has recently been implicated in mediating crucial cell fate decisions, either by limiting the time to reestablish lineage-determining epigenetic signatures (Dalton, 2015; Guo et al., 2014) or the transcription of developmentally relevant genes (Kueh et al., 2013; Singh et al., 2013). It is tempting to speculate that a similar mechanism might operate

to ensure the differentiation of CMPs into more terminal non-CMPs during the *"ultra-rapid"* rapid cell cycle phases of $CD8^+$ T cells. The experimental approaches introduced in this study could thus lay the groundwork for further elucidating the concerted molecular regulation of the cell cycle and distinct differentiation programs in developing immune cell populations.

5.3. Revisiting the autopilot model of antigen-independent T cell proliferation

The DC+*L.m.* vaccination approach, applied in this study, allowed us to further investigate the role of sustained antigen availability in regulating the cell cycle activities of emerging $CD8^+$ T cell subsets directly *in vivo*. This was achieved by rapidly killing peptide-pulsed DCs via a DTR-transgene, expressed under control of the CD11c-promotor (Jung et al., 2002), while leaving *L.m.*-induced inflammatory stimuli largely intact (Prlic et al., 2006). Interestingly, we found that all responding $CD8^+$ T cells continued to proliferate, even when depleting DCs at 48 hours after immunization. However, CMPs markedly slowed down their cell cycle in absence of antigen, whereas non-CMPs remained better poised to maintain their fast division speeds.

Our results shed new light on the antigen-independent proliferation of recently-activated $CD8^+$ T cell populations: on the one hand, elegant studies have demonstrated that short priming periods of 2-24 hours *in vitro* suffice to program multiple rounds of cell division, as well as effector and memory T cell differentiation, following antigen withdrawal or upon adoptive transfer into antigen-free recipients *in vivo (*Kaech et al., 2001; van Stipdonk et al., 2003; van Stipdonk et al., 2001). This suggested that important features of the $CD8^+$ T cell response are executed in complete absence of further antigenic stimulation, or in simplified terms, on *'autopilot'* (Bevan et al., 2001). On the other hand, subsequent studies have investigated the programming of $CD8^+$ T cell responses entirely *in vivo* and found that optimal proliferation, but not the functionality of accumulating effector or memory T cells, critically depended on the continued presence of antigenic signals for at least 2-4 days beyond initial activation (Blair et al., 2011; Prlic et al., 2006; Tewari et al., 2006). However, a comprehensive understanding of the regulatory events leading to this altered division activity has so far been lacking.

Our discovery of an antigen-dependent cell cycle regulation in emerging $CD8^+$ T cell subsets resolves this issue and serves to further refine the classic autopilot model of antigen-independent T cell proliferation. Based on the pronounced slow-down of the CMP cell cycle, we argue in

favor of a *'differential-autopilot'* that operates strongly in non-CMPs, but more weakly in CMPs. This concept thus incorporates important, but previously unappreciated differences in antigen-receptivity of acutely and long-term protective $CD8^+$ T cell subsets.

A temporal integration of antigenic stimuli has further been implicated in scaling the $CD8^+$ T cell response according to the immediate level of the pathogenic threat (Mayya et al., 2016; Tscharke et al., 2015). According to our analyses, it should be considered that such signal-integration occurs most strongly on the level of responding CMP cells. This proposition is of particular interest with regard to the progressive developmental order of CMPs, EMPs, and TEs, derived from our single cell fate mapping experiments. By placing CMPs at the top of the developmental hierarchy, an impaired CMP proliferation will thus eventually also propagate into the reduced output of its downstream EMP and TE descendants. It could therefore be speculated that an integration of antigenic stimuli acts to scale the response magnitude of activated $CD8^+$ T cells in a subset-dependent manner, from the top down.

5.4. Versatile role of IL-2 in the development of effector $CD8^+$ T cell subsets

We hypothesized that the distinct cell cycle speeds of CMPs and non-CMPs, in presence or absence of antigen, derived from subset-specific differences in receptivity to TCR-independent growth signals. Interestingly, an important role for IL-2 has been described in enhancing the antigen-independent proliferation of briefly-activated $CD8^+$ T cells *in vitro* (Kaech et al., 2001; van Stipdonk et al., 2003). However, the requirements for IL-2 signaling *in vivo* appear far more complex and its role in amplifying T cell proliferation has remained somewhat controversial (Wong et al., 2004). Recently, it could be demonstrated that prolonged expression of the high-affinity IL-2-receptor alpha-chain (CD25) facilitates the differentiation of effector $CD8^+$ T cells (Kalia et al., 2010) and prolongs division activity towards the later stages of the clonal expansion phase (Obar et al., 2010b; Starbeck-Miller et al., 2014).

In response to DC+*L.m.* vaccination, we found that only non-CMPs retained substantial CD25-expression-levels at day four and that this pattern clearly contributed to shaping the faster cell cycle speeds of this subset. Induction of CD25 depended on the availability of inflammatory cytokines, such as IL-12, that were associated with the *L.m.*-infection in our vaccination scheme. In contrast, depletion of antigen-presenting DCs had no effect on the CD25-expression profiles

of CMPs and non-CMPs, arguing that host cells likely represented the cellular origin of these cytokines, in line with previous observations (Cui et al., 2009). It should, however, be noted that the differences in cell cycle speed between CMPs and non-CMPs were not completely abolished in absence of CD25. This suggests that additional inflammation-dependent or -independent cues may be relevant for enforcing the faster cell cycles of non-CMPs.

Nonetheless, our findings reveal a relevant and previously unappreciated role for IL-2-signaling in promoting the cell cycle progression of developing effector $CD8^+$ T cell subsets *in vivo*. Earlier reports have established an IL-2-dependent acceleration of the G1/S-transition in cultured T cell lines (Appleman et al., 2000), via the PI3K-E2F pathway (Brennan et al., 1997). This mechanism could explain the shorter G1 phases, identified for ($CD25^{high}$) non-CMP cells in our work. The reduced IL-2-receptivity of ($CD25^{low}$) CMPs would in turn render this subset more dependent on sustained antigenic signaling for maintaining its division speed. In sum, these data shed new light on the biological roles of IL-2, by establishing its importance in promoting faster cell cycle speeds of effector $CD8^+$ T cells, in addition to facilitating their initial differentiation.

5.5. Implications for $CD8^+$ T cell memory and vaccine design

Memory $CD8^+$ T cells are critical for providing enhanced responsiveness to recurrent infections with previously encountered pathogens (Buchholz et al., 2016; Williams et al., 2007). Over the last decades, it has become clear that both the quantity and quality of memory T cells together determine the durability of long-term immune protection (Buchholz et al., 2016; Jameson et al., 2009; Kaech et al., 2002; Schmidt et al., 2008). Thus, antigen-specific memory T cells are typically present at higher frequencies than their naïve T cell precursors. Moreover, distinct subsets of memory T cells develop that differ in their capacity to mount efficient recall responses.

The ($CD62L^+$) CM subset, in particular, displays a superior capacity for long-term *in vivo* persistence as well as secondary re-expansion upon systemic challenge (Wherry et al., 2003). Elegant work, using serial transfers of single $CD8^+$ T-CM cells, has further revealed that this subset shares typical features of adult stem cells, such as the ability fo self-renew and the potency to differentiate into diverse effector T cell offspring (Graef et al., 2014). The results presented in this study describe novel aspects in the development of this stem-like T-CM subset:

on the one hand, we establish that slower cell cycle speeds constitute a distinguishing feature of emerging CMP cells, compared to their more terminal effector T cell descendants. On the other hand, we found that sustained antigen availability appears critical for maintaining optimal division speeds of CMPs throughout a primary T cell response, and thus contributes to expanding sufficient quantities of long-lived CM cells.

In the context of an acute infection, this indicates that rapid pathogen control will result in a smaller pool of accumulating T-CM cells. A protracted antigen-display, as described in various infection settings, will conversely help to expand a larger memory $CD8^+$ T cell pool. Similar considerations can be applied with regard to the composition of $CD8^+$ T cell-based vaccines: a delayed antigen release, e.g. described for nanoparticle vaccines (Shen et al., 2006; Zhao et al., 2014), might elicit stronger memory $CD8^+$ T cell responses by better maintaining the division speeds of CMPs - however, if antigen depots disperse too quickly, less memory can be formed (Demento et al., 2012). Engineering vaccine formulations with optimized antigen kinetics may thus present a promising strategy to boost memory $CD8^+$ T cell numbers to protective levels.

6. Summary

CD8+ T cell immune responses to infection or vaccination are initiated upon rapid, antigen-driven proliferation of rare naïve precursors and culminate in the expansion of short-lived effector as well as long-lived memory subsets. A tightly regulated cell cycle is clearly essential for mediating the clonal expansion of activated T cell populations. However, it has so far remained unclear, whether emerging TE and MP subsets acquire distinct cell cycle activities throughout primary immune responses and how this process is influenced by the sustained availability of antigen or inflammation beyond priming.

In this study, single cell fate mapping was applied to investigate the developmental pathway of CD8+ T cells upon vaccination with peptide-pulsed DCs, in the context of an accompanying wild-type *L.m.* infection. By modeling the highly diverse expansion and differentiation patterns of individual T cell families, we propose that T cell development is accurately captured by a stochastic computational framework, characterized by subset-specific proliferation and differentiation rates. According to this model, naïve T cells first differentiate into slowly-cycling CMPs, and then progressively into more rapid EMPs, and TEs. We directly measured the cell cycle activities of these emerging T cell subsets during the early stages of clonal expansion, by using time-resolved nucleoside analogue and DNA content labelling. Our results indicate that CMPs, characterized by a delayed progression through G1, indeed adopted substantially slower cell cycle speeds than their downstream (non-CMP) effector subsets.

In addition, premature depletion of antigen-presenting DCs revealed a further, strongly pronounced slow-down of the CMP cell cycle. In contrast, non-CMPs were better poised to maintain fast cell cycle speeds in absence of antigen and displayed enhanced responsiveness to high-affinity IL-2-signaling. This differential IL-2-receptivity clearly contributed to shaping the distinct proliferation rates of emerging CD8+ T cell subsets and was regulated by the sustained presence of inflammatory cytokines, induced by the accompanying *L.m.* infection.

Collectively, this work establishes a crucial proliferative hierarchy among emerging CD8+ T cell subsets that is fine-tuned by the sustained availability of antigen and inflammation throughout primary expansion. In line with an antigen-dependent regulation of the CMP cell cycle, we demonstrate that sustained antigenic stimulation strongly benefits the optimal expansion and recall capacity of the memory CD8+ T cell compartment.

7. Bibliography

1. Akira, S. & Hemmi, H. Recognition of pathogen-associated molecular patterns by TLR family. *Immunology letters* **85**, 85-95 (2003).

2. Akondy, R.S., Fitch, M., Edupuganti, S., Yang, S., Kissick, H.T., Li, K.W., Youngblood, B.A., Abdelsamed, H.A., McGuire, D.J., Cohen, K.W., Alexe, G., Nagar, S., McCausland, M.M., Gupta, S., Tata, P., Haining, W.N., McElrath, M.J., Zhang, D., Hu, B., Greenleaf, W.J., Goronzy, J.J., Mulligan, M.J., Hellerstein, M. & Ahmed, R. Origin and differentiation of human memory CD8 T cells after vaccination. *Nature* (2017).

3. Appay, V., Douek, D.C. & Price, D.A. CD8+ T cell efficacy in vaccination and disease. *Nature medicine* **14**, 623 (2008).

4. Appleman, L.J., Berezovskaya, A., Grass, I. & Boussiotis, V.A. CD28 costimulation mediates T cell expansion via IL-2-independent and IL-2-dependent regulation of cell cycle progression. *The Journal of Immunology* **164**, 144-151 (2000).

5. Arsenio, J., Kakaradov, B., Metz, P.J., Kim, S.H., Yeo, G.W. & Chang, J.T. Early specification of CD8+ T lymphocyte fates during adaptive immunity revealed by single-cell gene-expression analyses. *Nat Immunol* **15**, 365-372 (2014).

6. Badovinac, V.P. & Harty, J.T. Programming, demarcating, and manipulating CD8+ T-cell memory. *Immunological reviews* **211**, 67-80 (2006).

7. Badovinac, V.P., Messingham, K.A., Jabbari, A., Haring, J.S. & Harty, J.T. Accelerated CD8+ T-cell memory and prime-boost response after dendritic-cell vaccination. *Nat Med* **11**, 748-756 (2005).

8. Beltman, J.B., Marée, A.F.M., Lynch, J.N., Miller, M.J. & de Boer, R.J. Lymph node topology dictates T cell migration behavior. *The Journal of Experimental Medicine* **204**, 771-780 (2007).

9. Bertoletti, A. & Maini, M.K. Protection or damage: a dual role for the virus-specific cytotoxic T lymphocyte response in hepatitis B and C infection? *Current opinion in immunology* **12**, 403-408 (2000).

10. Bevan, M.J. & Fink, P.J. The CD8 response on autopilot. *Nat Immunol* **2**, 381-382 (2001).

11. Blair, D.A., Turner, D.L., Bose, T.O., Pham, Q.M., Bouchard, K.R., Williams, K.J., McAleer, J.P., Cauley, L.S., Vella, A.T. & Lefrancois, L. Duration of Antigen Availability Influences the Expansion and Memory Differentiation of T Cells. *The Journal of Immunology* **187**, 2310-2321 (2011).

12. Blattman, J.N., Antia, R., Sourdive, D.J., Wang, X., Kaech, S.M., Murali-Krishna, K., Altman, J.D. & Ahmed, R. Estimating the precursor frequency of naive antigen-specific CD8 T cells. *The Journal of experimental medicine* **195**, 657-664 (2002).

13. Bousso, P. & Robey, E. Dynamics of CD8+ T cell priming by dendritic cells in intact lymph nodes. *Nat Immunol* **4**, 579-585 (2003).

14. Brennan, P., Babbage, J.W., Burgering, B.M., Groner, B., Reif, K. & Cantrell, D.A. Phosphatidylinositol 3-kinase couples the interleukin-2 receptor to the cell cycle regulator E2F. *Immunity* **7**, 679-689 (1997).

15. Buchholz, V.R., Flossdorf, M., Hensel, I., Kretschmer, L., Weissbrich, B., Graf, P., Verschoor, A., Schiemann, M., Hofer, T. & Busch, D.H. Disparate individual fates compose robust CD8+ T cell immunity. *Science* **340**, 630-635 (2013a).

16. Buchholz, V.R., Gräf, P. & Busch, D.H. The smallest unit: effector and memory CD8+ T cell differentiation on the single cell level. *Frontiers in immunology* **4**, 31 (2013b).

17. Buchholz, V.R., Schumacher, T.N. & Busch, D.H. T Cell Fate at the Single-Cell Level. *Annu Rev Immunol* **34**, 65-92 (2016).

18. Burnet, S.F.M. The clonal selection theory of acquired immunity. (1959).

19. Busch, D.H., Fräßle, S.P., Sommermeyer, D., Buchholz, V.R. & Riddell, S.R. Role of memory T cell subsets for adoptive immunotherapy. Seminars in immunology; 2016: Elsevier; 2016. p. 28-34.

20. Cho, Y.L., Flossdorf, M., Kretschmer, L., Hofer, T., Busch, D.H. & Buchholz, V.R. TCR Signal Quality Modulates Fate Decisions of Single CD4(+) T Cells in a Probabilistic Manner. *Cell Rep* **20**, 806-818 (2017).

21. Cockburn, I.A., Chen, Y.-C., Overstreet, M.G., Lees, J.R., Van Rooijen, N., Farber, D.L. & Zavala, F. Prolonged antigen presentation is required for optimal CD8+ T cell responses against malaria liver stage parasites. *PLoS pathogens* **6**, e1000877 (2010).

22. Cousens, L.P., Peterson, R., Hsu, S., Dorner, A., Altman, J.D., Ahmed, R. & Biron, C.A. Two Roads Diverged: Interferon α/β– and Interleukin 12–mediated Pathways in Promoting T Cell Interferon γ Responses during Viral Infection. *The Journal of Experimental Medicine* **189**, 1315-1328 (1999).

23. Cui, W., Joshi, N.S., Jiang, A. & Kaech, S.M. Effects of Signal 3 during CD8 T cell priming: Bystander production of IL-12 enhances effector T cell expansion but promotes terminal differentiation. *Vaccine* **27**, 2177-2187 (2009).

24. Dalton, S. Linking the cell cycle to cell fate decisions. *Trends in cell biology* **25**, 592-600 (2015).

25. de Jager, W., Bourcier, K., Rijkers, G.T., Prakken, B.J. & Seyfert-Margolis, V. Prerequisites for cytokine measurements in clinical trials with multiplex immunoassays. *BMC Immunol* **10**, 52 (2009).

26. Demento, S.L., Cui, W., Criscione, J.M., Stern, E., Tulipan, J., Kaech, S.M. & Fahmy, T.M. Role of sustained antigen release from nanoparticle vaccines in shaping the T cell memory phenotype. *Biomaterials* **33**, 4957-4964 (2012).

27. Dowling, M.R., Kan, A., Heinzel, S., Zhou, J.H., Marchingo, J.M., Wellard, C.J., Markham, J.F. & Hodgkin, P.D. Stretched cell cycle model for proliferating lymphocytes. *Proc Natl Acad Sci U S A* **111**, 6377-6382 (2014).

28. Fearon, D.T. & Locksley, R.M. The instructive role of innate immunity in the acquired immune response. *Science* **272**, 50-54 (1996).

29. Gerlach, C., Rohr, J.C., Perie, L., van Rooij, N., van Heijst, J.W., Velds, A., Urbanus, J., Naik, S.H., Jacobs, H., Beltman, J.B., de Boer, R.J. & Schumacher, T.N. Heterogeneous differentiation patterns of individual CD8+ T cells. *Science* **340**, 635-639 (2013).

30. Gerlach, C., van Heijst, J.W., Swart, E., Sie, D., Armstrong, N., Kerkhoven, R.M., Zehn, D., Bevan, M.J., Schepers, K. & Schumacher, T.N. One naive T cell, multiple fates in CD8+ T cell differentiation. *Journal of Experimental Medicine* **207**, 1235-1246 (2010).

31. Gett, A.V. & Hodgkin, P.D. A cellular calculus for signal integration by T cells. *Nature immunology* **1**, 239 (2000).

32. Gitlin, A.D., Mayer, C.T., Oliveira, T.Y., Shulman, Z., Jones, M.J., Koren, A. & Nussenzweig, M.C. T cell help controls the speed of the cell cycle in germinal center B cells. *Science* **349**, 643-646 (2015).

33. Gitlin, A.D., Shulman, Z. & Nussenzweig, M.C. Clonal selection in the germinal centre by regulated proliferation and hypermutation. *Nature* **509**, 637-640 (2014).

34. Goldrath, A.W. & Bevan, M.J. Selecting and maintaining a diverse T-cell repertoire. *Nature* **402**, 255 (1999).

35. Gookin, S., Min, M., Phadke, H., Chung, M., Moser, J., Miller, I., Carter, D. & Spencer, S.L. A map of protein dynamics during cell-cycle progression and cell-cycle exit. *PLoS biology* **15**, e2003268 (2017).

36. Graef, P., Buchholz, V.R., Stemberger, C., Flossdorf, M., Henkel, L., Schiemann, M., Drexler, I., Hofer, T., Riddell, S.R. & Busch, D.H. Serial transfer of single-cell-derived immunocompetence reveals stemness of CD8(+) central memory T cells. *Immunity* **41**, 116-126 (2014).

37. Guo, S., Zi, X., Schulz, V.P., Cheng, J., Zhong, M., Koochaki, S.H., Megyola, C.M., Pan, X., Heydari, K. & Weissman, S.M. Nonstochastic reprogramming from a privileged somatic cell state. *Cell* **156**, 649-662 (2014).

38. Haring, J.S., Badovinac, V.P. & Harty, J.T. Inflaming the CD8+ T cell response. *Immunity* **25**, 19-29 (2006).

39. Harty, J.T. & Badovinac, V.P. Shaping and reshaping CD8+ T-cell memory. *Nature Reviews Immunology* **8**, 107-119 (2008).

40. Heath, W.R., Belz, G.T., Behrens, G.M., Smith, C.M., Forehan, S.P., Parish, I.A., Davey, G.M., Wilson, N.S., Carbone, F.R. & Villadangos, J.A. Cross-presentation, dendritic cell

subsets, and the generation of immunity to cellular antigens. *Immunological reviews* **199**, 9-26 (2004).

41. Heinzel, S., Binh Giang, T., Kan, A., Marchingo, J.M., Lye, B.K., Corcoran, L.M. & Hodgkin, P.D. A Myc-dependent division timer complements a cell-death timer to regulate T cell and B cell responses. *Nat Immunol* **18**, 96-103 (2017).

42. Hendriks, J., Gravestein, L.A., Tesselaar, K., van Lier, R.A., Schumacher, T.N. & Borst, J. CD27 is required for generation and long-term maintenance of T cell immunity. *Nature immunology* **1**, 433 (2000).

43. Hikono, H., Kohlmeier, J.E., Takamura, S., Wittmer, S.T., Roberts, A.D. & Woodland, D.L. Activation phenotype, rather than central–or effector–memory phenotype, predicts the recall efficacy of memory CD8+ T cells. *Journal of Experimental Medicine* **204**, 1625-1636 (2007).

44. Huster, K.M., Busch, V., Schiemann, M., Linkemann, K., Kerksiek, K.M., Wagner, H. & Busch, D.H. Selective expression of IL-7 receptor on memory T cells identifies early CD40L-dependent generation of distinct CD8+ memory T cell subsets. *Proceedings of the National Academy of Sciences* **101**, 5610-5615 (2004).

45. Iwasaki, A. & Medzhitov, R. Control of adaptive immunity by the innate immune system. *Nature immunology* **16**, 343 (2015).

46. Jameson, S.C. & Masopust, D. Diversity in T cell memory: an embarrassment of riches. *Immunity* **31**, 859-871 (2009).

47. Joshi, N.S., Cui, W., Chandele, A., Lee, H.K., Urso, D.R., Hagman, J., Gapin, L. & Kaech, S.M. Inflammation directs memory precursor and short-lived effector CD8(+) T cell fates via the graded expression of T-bet transcription factor. *Immunity* **27**, 281-295 (2007).

48. Jung, S., Unutmaz, D., Wong, P., Sano, G., De los Santos, K., Sparwasser, T., Wu, S., Vuthoori, S., Ko, K., Zavala, F., Pamer, E.G., Littman, D.R. & Lang, R.A. In vivo depletion of CD11c+ dendritic cells abrogates priming of CD8+ T cells by exogenous cell-associated antigens. *Immunity* **17**, 211-220 (2002).

49. Kaech, S.M. & Ahmed, R. Memory CD8+ T cell differentiation: initial antigen encounter triggers a developmental program in naive cells. *Nat Immunol* **2**, 415-422 (2001).

50. Kaech, S.M. & Cui, W. Transcriptional control of effector and memory CD8+ T cell differentiation. *Nat Rev Immunol* **12**, 749-761 (2012).

51. Kaech, S.M., Tan, J.T., Wherry, E.J., Konieczny, B.T., Surh, C.D. & Ahmed, R. Selective expression of the interleukin 7 receptor identifies effector CD8 T cells that give rise to long-lived memory cells. *Nature immunology* **4**, 1191 (2003).

52. Kaech, S.M., Wherry, E.J. & Ahmed, R. Vaccines: effector and memory T-cell differentiation: implications for vaccine development. *Nature Reviews Immunology* **2**, 251 (2002).

53. Kakaradov, B., Arsenio, J., Widjaja, C.E., He, Z., Aigner, S., Metz, P.J., Yu, B., Wehrens, E.J., Lopez, J., Kim, S.H., Zuniga, E.I., Goldrath, A.W., Chang, J.T. & Yeo, G.W. Early transcriptional and epigenetic regulation of CD8(+) T cell differentiation revealed by single-cell RNA sequencing. *Nat Immunol* **18**, 422-432 (2017).

54. Kalia, V., Sarkar, S., Subramaniam, S., Haining, W.N., Smith, K.A. & Ahmed, R. Prolonged interleukin-2Ralpha expression on virus-specific CD8+ T cells favors terminal-effector differentiation in vivo. *Immunity* **32**, 91-103 (2010).

55. Kim, S.Y., Herbst, A., Tworkowski, K.A., Salghetti, S.E. & Tansey, W.P. Skp2 regulates Myc protein stability and activity. *Mol Cell* **11**, 1177-1188 (2003).

56. Kim, T.S., Hufford, M.M., Sun, J., Fu, Y.-X. & Braciale, T.J. Antigen persistence and the control of local T cell memory by migrant respiratory dendritic cells after acute virus infection. *Journal of Experimental Medicine* **207**, 1161-1172 (2010).

57. Kinjyo, I., Qin, J., Tan, S.Y., Wellard, C.J., Mrass, P., Ritchie, W., Doi, A., Cavanagh, L.L., Tomura, M., Sakaue-Sawano, A., Kanagawa, O., Miyawaki, A., Hodgkin, P.D. & Weninger, W. Real-time tracking of cell cycle progression during CD8+ effector and memory T-cell differentiation. *Nat Commun* **6**, 6301 (2015).

58. Klebanoff, C.A., Gattinoni, L. & Restifo, N.P. CD8+ T-cell memory in tumor immunology and immunotherapy. *Immunological reviews* **211**, 214-224 (2006).

59. Klebanoff, C.A., Gattinoni, L. & Restifo, N.P. Sorting through subsets: which T cell populations mediate highly effective adoptive immunotherapy? *Journal of immunotherapy (Hagerstown, Md.: 1997)* **35**, 651 (2012).

60. Kretschmer, L., Flossdorf, M., Mir, J., Cho, Y.-L., Plambeck, M., Treise, I., Toska, A., Heinzel, S., Schiemann, M., Busch, D.H. & Buchholz, V.R. Differential expansion of T central memory precursor and effector subsets is regulated by division speed. *Nature Communications* **11**, 113 (2020).

61. Ku, C.C., Murakami, M., Sakamoto, A., Kappler, J. & Marrack, P. Control of homeostasis of CD8+ memory T cells by opposing cytokines. *Science* **288**, 675-678 (2000).

62. Kueh, H.Y., Champhekar, A., Nutt, S.L., Elowitz, M.B. & Rothenberg, E.V. Positive feedback between PU. 1 and the cell cycle controls myeloid differentiation. *Science* **341**, 670-673 (2013).

63. Lanzavecchia, A. & Sallusto, F. Dynamics of T lymphocyte responses: intermediates, effectors, and memory cells. *Science* **290**, 92-97 (2000).

64. Lau, L.L., Jamieson, B.D., Somasundaram, T. & Ahmed, R. Cytotoxic T-cell memory without antigen. *Nature* **369**, 648 (1994).

65. Liboska, R., Ligasova, A., Strunin, D., Rosenberg, I. & Koberna, K. Most anti-BrdU antibodies react with 2'-deoxy-5-ethynyluridine -- the method for the effective suppression of this cross-reactivity. *PLoS One* **7**, e51679 (2012).

66. Livingstone, A.M. & Kuhn, M. Peptide-pulsed splenic dendritic cells prime long-lasting CD8(+) T cell memory in the absence of cross-priming by host APC. *Eur J Immunol* **32**, 281-290 (2002).

67. Marchingo, J.M., Kan, A., Sutherland, R.M., Duffy, K.R., Wellard, C.J., Belz, G.T., Lew, A.M., Dowling, M.R., Heinzel, S. & Hodgkin, P.D. Antigen affinity, costimulation, and cytokine inputs sum linearly to amplify T cell expansion. *Science* **346**, 1123-1127 (2014).

68. Marchingo, J.M., Prevedello, G., Kan, A., Heinzel, S., Hodgkin, P.D. & Duffy, K.R. T-cell stimuli independently sum to regulate an inherited clonal division fate. *Nat Commun* **7**, 13540 (2016).

69. Matiašová, A., Ševc, J., Mikeš, J., Jendželovský, R., Daxnerová, Z. & Fedoročko, P. Flow cytometric determination of 5-bromo-2′-deoxyuridine pharmacokinetics in blood serum

after intraperitoneal administration to rats and mice. *Histochemistry and cell biology* **142**, 703-712 (2014).

70. Mayya, V. & Dustin, M.L. What Scales the T Cell Response? *Trends Immunol* **37**, 513-522 (2016).

71. Mescher, M.F., Curtsinger, J.M., Agarwal, P., Casey, K.A., Gerner, M., Hammerbeck, C.D., Popescu, F. & Xiao, Z. Signals required for programming effector and memory development by CD8+ T cells. *Immunological reviews* **211**, 81-92 (2006).

72. Miller, I., Min, M., Yang, C., Tian, C., Gookin, S., Carter, D. & Spencer, S.L. Ki67 is a Graded Rather than a Binary Marker of Proliferation versus Quiescence. *Cell Rep* **24**, 1105-1112 e1105 (2018).

73. Moser, J., Miller, I., Carter, D. & Spencer, S.L. Control of the Restriction Point by Rb and p21. *Proceedings of the National Academy of Sciences* **115**, E8219-E8227 (2018).

74. Nunez, R. DNA measurement and cell cycle analysis by flow cytometry. *Current issues in molecular biology* **3**, 67-70 (2001).

75. Obar, J.J. & Lefrançois, L. Memory CD8+ T cell differentiation. *Annals of the New York Academy of Sciences* **1183**, 251 (2010a).

76. Obar, J.J., Molloy, M.J., Jellison, E.R., Stoklasek, T.A., Zhang, W., Usherwood, E.J. & Lefrançois, L. CD4+ T cell regulation of CD25 expression controls development of short-lived effector CD8+ T cells in primary and secondary responses. *Proceedings of the National Academy of Sciences* **107**, 193-198 (2010b).

77. Pipkin, M.E., Sacks, J.A., Cruz-Guilloty, F., Lichtenheld, M.G., Bevan, M.J. & Rao, A. Interleukin-2 and inflammation induce distinct transcriptional programs that promote the differentiation of effector cytolytic T cells. *Immunity* **32**, 79-90 (2010).

78. Prlic, M., Hernandez-Hoyos, G. & Bevan, M.J. Duration of the initial TCR stimulus controls the magnitude but not functionality of the CD8+ T cell response. *J Exp Med* **203**, 2135-2143 (2006).

79. Reiner, S.L. Development in motion: helper T cells at work. *Cell* **129**, 33-36 (2007).

80. Rosenberg, S.A., Restifo, N.P., Yang, J.C., Morgan, R.A. & Dudley, M.E. Adoptive cell transfer: a clinical path to effective cancer immunotherapy. *Nature Reviews Cancer* **8**, 299 (2008).

81. Russell, J.H. & Ley, T.J. Lymphocyte-mediated cytotoxicity. *Annual review of immunology* **20**, 323-370 (2002).

82. Sakaue-Sawano, A., Kurokawa, H., Morimura, T., Hanyu, A., Hama, H., Osawa, H., Kashiwagi, S., Fukami, K., Miyata, T. & Miyoshi, H. Visualizing spatiotemporal dynamics of multicellular cell-cycle progression. *Cell* **132**, 487-498 (2008).

83. Sallusto, F., Geginat, J. & Lanzavecchia, A. Central memory and effector memory T cell subsets: function, generation, and maintenance. *Annu. Rev. Immunol.* **22**, 745-763 (2004).

84. Sallusto, F., Lanzavecchia, A., Araki, K. & Ahmed, R. From vaccines to memory and back. *Immunity* **33**, 451-463 (2010).

85. Sallusto, F., Lenig, D., Förster, R., Lipp, M. & Lanzavecchia, A. Two subsets of memory T lymphocytes with distinct homing potentials and effector functions. *Nature* **401**, 708 (1999).

86. Sarkar, S., Kalia, V., Haining, W.N., Konieczny, B.T., Subramaniam, S. & Ahmed, R. Functional and genomic profiling of effector CD8 T cell subsets with distinct memory fates. *J Exp Med* **205**, 625-640 (2008).

87. Schlub, T.E., Venturi, V., Kedzierska, K., Wellard, C., Doherty, P.C., Turner, S.J., Ribeiro, R.M., Hodgkin, P.D. & Davenport, M.P. Division-linked differentiation can account for CD8+ T-cell phenotype in vivo. *European journal of immunology* **39**, 67-77 (2009).

88. Schluns, K.S., Kieper, W.C., Jameson, S.C. & Lefrançois, L. Interleukin-7 mediates the homeostasis of naive and memory CD8 T cells in vivo. *Nature immunology* **1**, 426 (2000).

89. Schmidt, N.W., Podyminogin, R.L., Butler, N.S., Badovinac, V.P., Tucker, B.J., Bahjat, K.S., Lauer, P., Reyes-Sandoval, A., Hutchings, C.L. & Moore, A.C. Memory CD8 T cell responses exceeding a large but definable threshold provide long-term immunity to malaria. *Proceedings of the National Academy of Sciences* **105**, 14017-14022 (2008).

90. Scholzen, T. & Gerdes, J. The Ki-67 protein: from the known and the unknown. *Journal of cellular physiology* **182**, 311-322 (2000).

91. Sharpe, A.H. & Freeman, G.J. The B7–CD28 superfamily. *Nature Reviews Immunology* **2**, 116 (2002).

92. Shen, H., Ackerman, A.L., Cody, V., Giodini, A., Hinson, E.R., Cresswell, P., Edelson, R.L., Saltzman, W.M. & Hanlon, D.J. Enhanced and prolonged cross-presentation following endosomal escape of exogenous antigens encapsulated in biodegradable nanoparticles. *Immunology* **117**, 78-88 (2006).

93. Singh, A.M., Chappell, J., Trost, R., Lin, L., Wang, T., Tang, J., Wu, H., Zhao, S., Jin, P. & Dalton, S. Cell-cycle control of developmentally regulated transcription factors accounts for heterogeneity in human pluripotent cells. *Stem cell reports* **1**, 532-544 (2013).

94. Smith, G.A., Uchida, K., Weiss, A. & Taunton, J. Essential biphasic role for JAK3 catalytic activity in IL-2 receptor signaling. *Nat Chem Biol* **12**, 373-379 (2016).

95. Spencer, S.L., Cappell, S.D., Tsai, F.-C., Overton, K.W., Wang, C.L. & Meyer, T. The proliferation-quiescence decision is controlled by a bifurcation in CDK2 activity at mitotic exit. *Cell* **155**, 369-383 (2013).

96. Sprent, J. & Surh, C.D. T cell memory. *Annual review of immunology* **20**, 551-579 (2002).

97. Starbeck-Miller, G.R., Xue, H.H. & Harty, J.T. IL-12 and type I interferon prolong the division of activated CD8 T cells by maintaining high-affinity IL-2 signaling in vivo. *J Exp Med* **211**, 105-120 (2014).

98. Starr, T.K., Jameson, S.C. & Hogquist, K.A. Positive and negative selection of T cells. *Annu Rev Immunol* **21**, 139-176 (2003).

99. Steinman, R.M. The dendritic cell system and its role in immunogenicity. *Annu Rev Immunol* **9**, 271-296 (1991).

100. Stemberger, C., Huster, K.M., Koffler, M., Anderl, F., Schiemann, M., Wagner, H. & Busch, D.H. A single naive CD8+ T cell precursor can develop into diverse effector and memory subsets. *Immunity* **27**, 985-997 (2007).

101. Strugnell, R.A. & Wijburg, O.L. The role of secretory antibodies in infection immunity. *Nature Reviews Microbiology* **8**, 656 (2010).

102. Tewari, K., Walent, J., Svaren, J., Zamoyska, R. & Suresh, M. Differential requirement for Lck during primary and memory CD8+ T cell responses. *Proceedings of the National Academy of Sciences* **103**, 16388-16393 (2006).

103. Tonegawa, S. The molecules of the immune system. *Sci Am* **253**, 122-131 (1985).

104. Tscharke, D.C., Croft, N.P., Doherty, P.C. & La Gruta, N.L. Sizing up the key determinants of the CD8(+) T cell response. *Nat Rev Immunol* **15**, 705-716 (2015).

105. van Faassen, H., Dudani, R., Krishnan, L. & Sad, S. Prolonged antigen presentation, APC-, and CD8+ T cell turnover during mycobacterial infection: comparison with Listeria monocytogenes. *The Journal of Immunology* **172**, 3491-3500 (2004).

106. Van Parijs, L. & Abbas, A.K. Homeostasis and self-tolerance in the immune system: turning lymphocytes off. *Science* **280**, 243-248 (1998).

107. van Stipdonk, M.J., Hardenberg, G., Bijker, M.S., Lemmens, E.E., Droin, N.M., Green, D.R. & Schoenberger, S.P. Dynamic programming of CD8+ T lymphocyte responses. *Nat Immunol* **4**, 361-365 (2003).

108. van Stipdonk, M.J., Lemmens, E.E. & Schoenberger, S.P. Naive CTLs require a single brief period of antigenic stimulation for clonal expansion and differentiation. *Nat Immunol* **2**, 423-429 (2001).

109. Wherry, E.J., Teichgräber, V., Becker, T.C., Masopust, D., Kaech, S.M., Antia, R., Von Andrian, U.H. & Ahmed, R. Lineage relationship and protective immunity of memory CD8 T cell subsets. *Nature immunology* **4**, 225 (2003).

110. Williams, M.A. & Bevan, M.J. Effector and memory CTL differentiation. *Annu. Rev. Immunol.* **25**, 171-192 (2007).

111. Wong, P. & Pamer, E.G. Disparate in vitro and in vivo requirements for IL-2 during antigen-independent CD8 T cell expansion. *The Journal of Immunology* **172**, 2171-2176 (2004).

112. Yoon, H., Kim, T.S. & Braciale, T.J. The cell cycle time of CD8+ T cells responding in vivo is controlled by the type of antigenic stimulus. *PloS one* **5**, e15423 (2010).

113. Zammit, D.J., Turner, D.L., Klonowski, K.D., Lefrançois, L. & Cauley, L.S. Residual antigen presentation after influenza virus infection affects CD8 T cell activation and migration. *Immunity* **24**, 439-449 (2006).

114. Zhang, N. & Bevan, M.J. CD8+ T cells: foot soldiers of the immune system. *Immunity* **35**, 161-168 (2011).

115. Zhang, X., Sun, S., Hwang, I., Tough, D.F. & Sprent, J. Potent and selective stimulation of memory-phenotype CD8+ T cells in vivo by IL-15. *Immunity* **8**, 591-599 (1998).

116. Zhao, L., Seth, A., Wibowo, N., Zhao, C.-X., Mitter, N., Yu, C. & Middelberg, A.P. Nanoparticle vaccines. *Vaccine* **32**, 327-337 (2014).

117. Ziegler, S.F., Ramsdell, F. & Alderson, M.R. The activation antigen CD69. *Stem cells* **12**, 456-465 (1994).

118. Zinkernagel, R. & Doherty, P. Restriction of in vitro T cell-mediated cytotoxicity in lymphocytic choriomeningitis within a syngeneic or semiallogeneic system. (1974a).

119. Zinkernagel, R.M. & Doherty, P.C. Immunological surveillance against altered self components by sensitised T lymphocytes in lymphocytes choriomeningitis. *Nature* **251**, 547 (1974b).

8. Acknowledgements

The completion of this thesis relied on the continuous support from many important people throughout the course of this research.

First, I would like to express my deep gratitude to my supervisors Prof. Dr. Dirk Busch and Dr. Veit Buchholz, who devised the study and continuously supported me during the course of this project. The profound scientific discussions and valuable suggestions have greatly contributed to the success of this work. The academic guidance and the inspiring research environment, created in the laboratory, have further helped me to advance in my scientific and personal development. I am especially thankful for the various opportunities to attend high-profile conferences and to present my work to the broader scientific community.

I would also like to thank my mentors Prof. Dr. Admaar Verschoor and PD Dr. Hendrik Poeck for the advice and guidance they have given me. I would also like to extend my gratitude to PD Dr. Michael Quante, who initially pointed me towards applying for the doctoral program "Translational Medicine" at the Technische Universität München (TUM).

Numerous contributions of collaborators have helped to advance this project: the combined efforts of Dr. Michael Flossdorf and his Computational Modeling group, in particular Jonas Mir and Albulena Toska, clearly stand out. The theoretical framework for quantifying the cell cycles of activated $CD8^+$ T cells has greatly helped to elucidate fundamental biological processes in developing immune cell subsets. I would especially like to thank Dr. Susanne Heinzel for collaborating on this project and for supplying cell material. I further extend my thanks to Dr. Yi-Li Cho, Dr. Irina Treise, and Marten Plambeck for their support in performing experiments, as well as Katherine Molter and Inge Hensel for their help in organizing the lab and their work in the animal facility. Finally, I would like to acknowledge the efforts of Lynette Henkel, Corinne Angerpointner, and Immanuel Andrä in cell sorting, as well as Dr. Matthias Schiemann for his supervision of the Flow Cytometry Core facility (CyTUM).

Lastly, I am immensely grateful for the unwavering support of my family and friends. In particular, I would like to thank my parents Wolfgang and Angelika, my brothers Simon and Toby, as well as my girlfriend Andrea for believing in me and for supporting me in my studies.